signaling pathway in PC12 cells (Figure 2). Akt was 2-fold activated in both CM-BSO (–) and CM-BSO (+) treated PC12 cells, but no significant difference between the 2 groups was observed.

FGF2 and BMP2 are upregulated through p38 MAPK signaling in hADMPCs exposed to oxidative stress

We next examined which growth factors or cytokines from BSO-treated hADMPCs were involved in stimulation of neurite outgrowth. We found that both mRNA (Figure 3A and B) and protein (Figure 3C and D) levels for BMP2 and FGF2 were markedly increased in hADMPCs treated with BSO. To determine if this upregulation was caused by ROS, all cells were exposed to the antioxidant *N*-acetylcysteine (NAC). As we expected, addition of NAC to BSO-treated hADMPCs reduced the expression levels of BMP2 and FGF2 to control levels (Figure 3E and F). As BMP2 together with FGF2 has

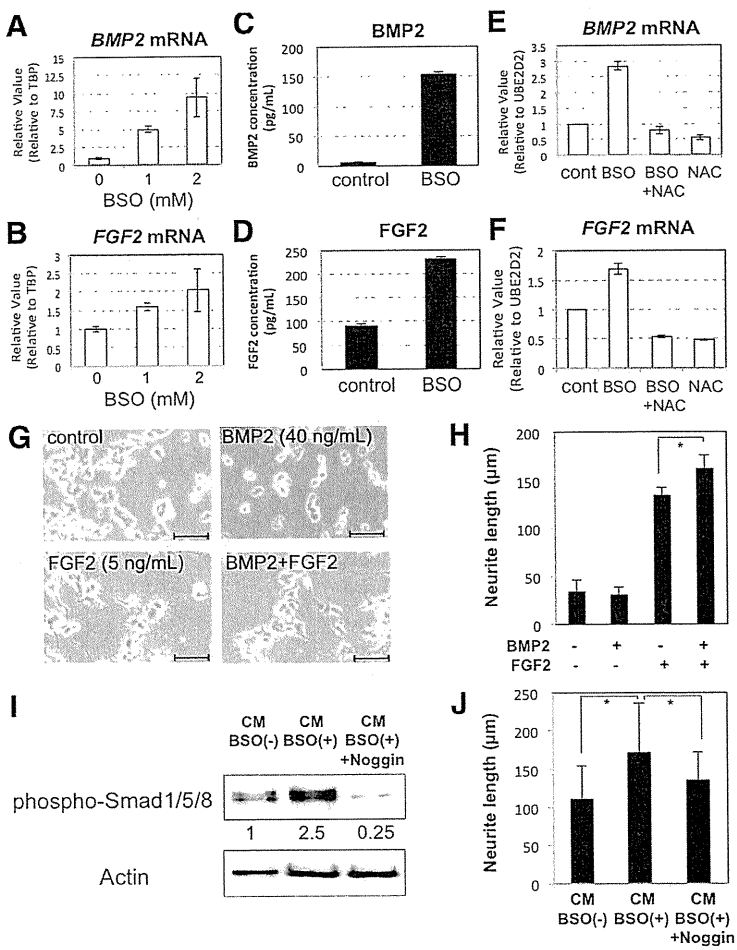

Figure 3 Transcription and secretion of BMP2 and FGF2 were increased in hADMPCs exposed to oxidative stress. (A, B) Upregulation of *BMP2* (**A**) and *FGF2* (**B**) mRNA in hADMPCs by BSO in a dose-dependent manner. **(C, D)** Secretion of BMP2 (**C**) and FGF2 (**D**) from hADMPCs in medium alone (cont) or with addition of 1 mM BSO (BSO) was analyzed by ELISA. **(E, F)** NAC treatment repressed the expression levels of *BMP2* and *FGF2* upregulated by BSO to the control levels. Expression of *BMP2* (E) and *FGF2* (F) mRNA was analyzed by q-PCR. cDNA was generated from total RNA extracted from hADMPCs (cont), hADMPCs treated with 1 mM BSO (BSO), 1 mM BSO + 5 mM NAC (BSO + NAC), and 5 mM NAC (NAC). The most reliable internal control gene was determined using the geNorm Software. **(G, H)** PC12 cells were cultured in differentiation medium alone (control), or differentiation medium supplemented with BMP2 (40 ng/mL), FGF2 (5 ng/mL), or both BMP2 and FGF2 (BMP2 + FGF2) for 2 days. (**G**) Representative images of neurite outgrowth in PC12 cells. Scale bars, 200 μm. (**H**) One hundred individual neurites were measured in each sample using Dynamic Cell Count Analyzer BZ-H1C (Keyence) and average neurite length was calculated. *, $P < 0.05$ (Student's t test). **(I, J)** PC12 cells were cultured in CM-BSO (–), CM-BSO (+), or CM-BSO (+) added with recombinant murine Noggin (200 ng/mL). **(I)** Western blot analysis of PC12 cells 1 h after CM treatment. Proteins extracted from each sample were resolved by SDS-PAGE, transferred to a membrane, and probed with anti-phosphorylated Smad1/5/8 (phospho-Smad1/5/8) and anti-Actin. Numbers below blots indicate relative band intensities as determined by the ImageJ software. (**J**) Two days after CM treatment, 100 individual neurites in PC12 cells were measured in each sample using Dynamic Cell Count Analyzer BZ-H1C (Keyence) and average neurite length was calculated. *, $P < 0.05$ (Student's t test).

previously been shown to induce neurite outgrowth in PC12 cells [26,27], we examined the effect of BMP2 and FGF2 on neurite outgrowth. We confirmed that PC12 cells did not differentiate effectively by BMP2 treatment alone, but BMP2 significantly augmented FGF2-induced neurite outgrowth in PC12 cells (Figure 3G and H), as previously reported. Moreover, in order to confirm the effect of BMP2 on neurite outgrowth in PC12 cells, 200 ng/mL of Noggin, an antagonist of BMP signaling, was added to CM-BSO(+). Addition of Noggin significantly suppressed the CM-BSO (+)-evoked phosphorylation of Smad1/5/8 (Figure 3I) and shortened the length of neurite outgrowth in PC12 cells (Figure 3J).

To address the question of which intracellular signaling pathways are affected by oxidative stress in hADMPCs, we focused on MAPK signaling since previous studies had suggested that accumulation of ROS in cells led to the activation of Erk1/2, p38, and JNK MAPK [28,29]. Western blotting revealed that BSO treatment markedly activated the p38 MAPK pathway; SB203580 could inhibit the activation, and U0126 treatment stimulated the activation (Figure 4A). ERK1/2 MAPK was significantly phosphorylated by BSO treatment, and ERK1/2 activation was reduced to the control level by treatment with U0126 (Figure 4B). In contrast, JNK activation was not observed in BSO-treated hADMPCs (Figure 4B). Therefore, we further investigated the relationship between increases in BMP2 and FGF2 expression and activation of the p38 and ERK1/2 MAPK signaling pathways by oxidative stress. Treatment

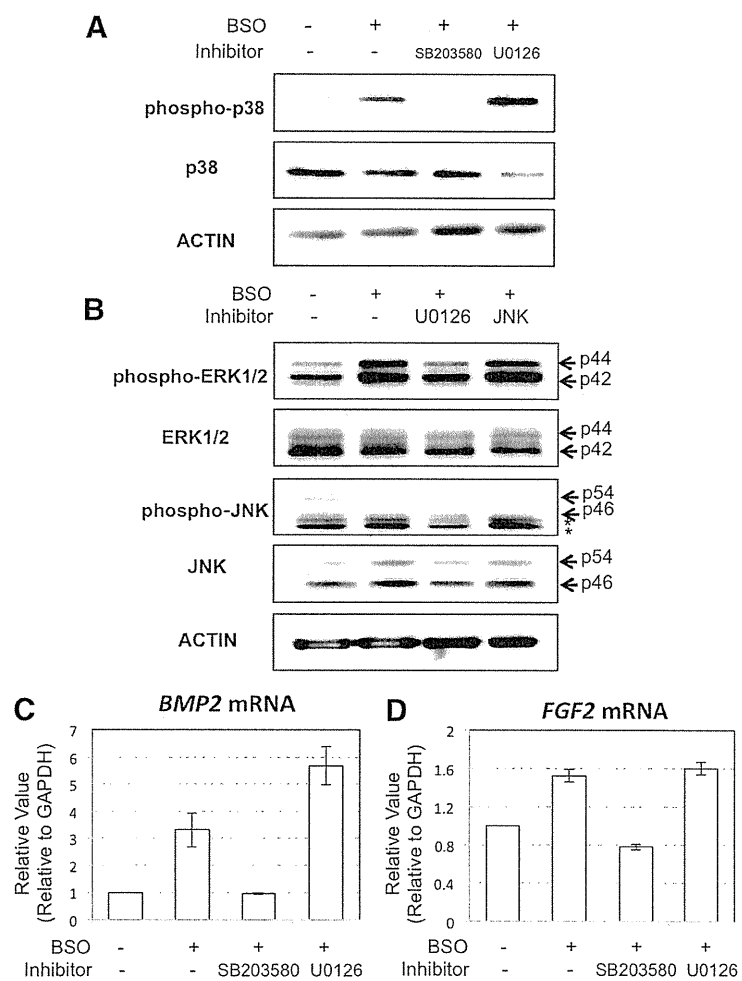

Figure 4 BMP2 and FGF2 were upregulated through activation of p38 MAPK. Inhibiton of p38 MAPK resulted in the supression of *BMP2* and *FGF2* transcripts upregulated by BSO treatment in hADMPCs. hADMPCs were pre-treated with 10 μM of SB203580, 10 μM of U0126 or 10 μM of JNK inhibitor II for 2 h followed by 1 mM BSO treatment for 16 h. The medium was replaced with fresh culture medium and the cells were cultured for another 2 days. **(A)** Western blot analysis of p38 MAPK activation in hADMPCs. **(B)** Western blot analysis of ERK1/2 MAPK, JNK SAPK activation in hADMPCs. **(C, D)** Transcription levels of *BMP2* (**C**) and *FGF2* (**D**) were analyzed by q-PCR. The most reliable internal control gene was determined using the geNorm Software.

with the p38 MAPK inhibitor SB203580 dramatically downregulated the expression levels of *BMP2* and *FGF2* to control levels (Figure 4C and D). In contrast, the Erk1/2 MAPK inhibitor U0126 had no effect on *FGF2* expression levels and led to a slight increase in *BMP2* expression (Figure 4C and D).

MKK6-mediated activation of p38 MAPK increases BMP2 and FGF2 expression in hADMPCs

To further confirm the involvement of p38 MAPK in the regulation of BMP2 and FGF2, hADMPCs were transduced with a lentiviral vector expressing constitutively active MKK6 (MKK6 (glu)) [30] from an EF1α promoter. As shown in Figure 5A, lentiviral transduction of MKK6 (glu) led to expression of Flag-tagged MKK6 (glu) in hADMPCs. Moreover, the expression of MKK6 (glu) resulted in activation of p38 MAPK as expected [30] (Figure 5A), and upregulation of BMP2 and FGF2 expression (Figure 5B-E).

NF-κB is not activated in hADMPCs exposed to oxidative stress

It has been reported that NF-κB directly binds to the *BMP2* promoter to induce its expression [31], and MSK1, a downstream molecule of p38 MAPK, is involved in NF-κB transactivation [32]. Therefore, we

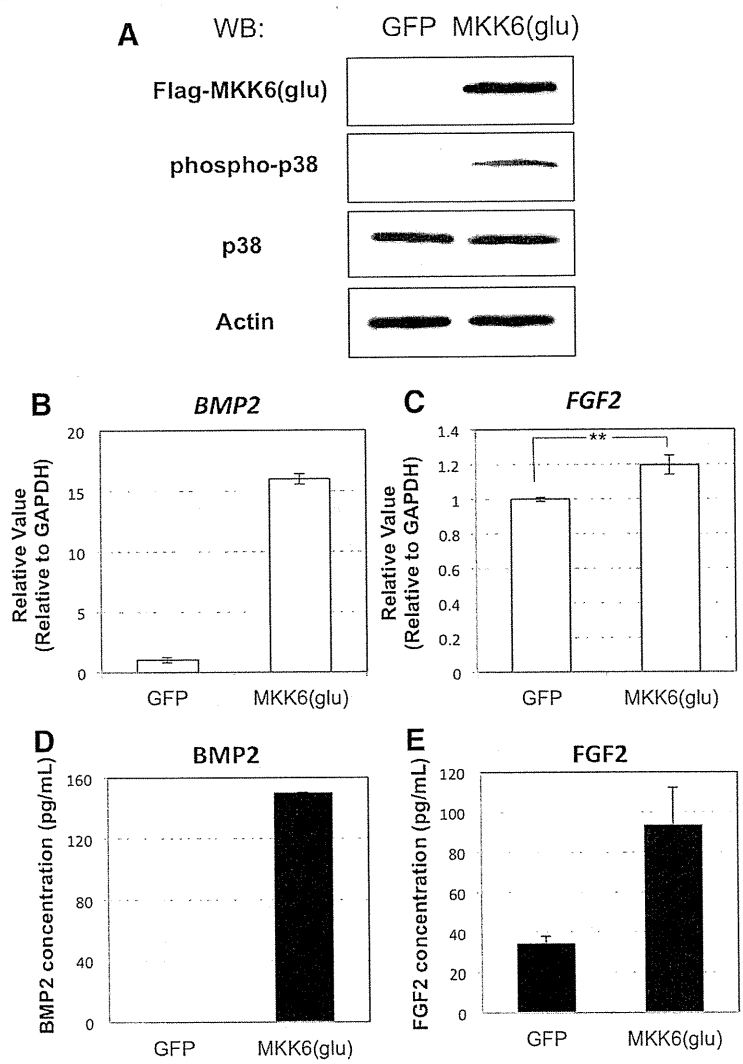

Figure 5 Activation of p38 MAPK by a constitutively active form of MKK6 resulted in elevated expression of BMP2 and FGF2. (A) A lentiviral vector expressing Flag-tagged MKK6 (glu) was transfected into hADMPCs. Expression of Flag-tagged MKK6 (glu), phosphorylated p38 MAPK and p38 MAPK was analyzed by western blotting. A CSII-EF-EGFP lentiviral vector was infected as a control (GFP). Actin was detected as an internal control. **(B, C)** Transcriptional levels of *BMP2* (**B**) and *FGF2* (**C**) were analyzed by q-PCR. The most reliable internal control gene was determined using the geNorm Software. **(D, E)** BMP2 (**D**) and FGF2 (**E**) secretion was analyzed by ELISA.

hypothesized that p38 MAPK-mediated activation of NF-κB might contribute to elevated expression of *BMP2* mRNA. To confirm this hypothesis, transcriptional activation of NF-κB was examined by measuring luciferase activity driven by the synthetic NF-κB response element. We found that transcriptional activity of NF-κB was not stimulated by BSO treatment (Figure 6A), and immunocytochemical analysis also revealed that NF-κB was not activated (nuclear localization of NF-κB/p65 was rarely observed) in BSO-treated hADMPCs (Figure 6B). These results suggested that elevated expression of *BMP2* mRNA is not mediated by NF-κB signaling.

Our current data thus demonstrate the crucial role of ROS, via activation of the p38 MAPK signaling pathway, in regulating expression levels of the neurotrophic factors BMP2 and FGF2 in hADMPCs. The overall model that we propose, based upon our findings, is shown in Figure 7.

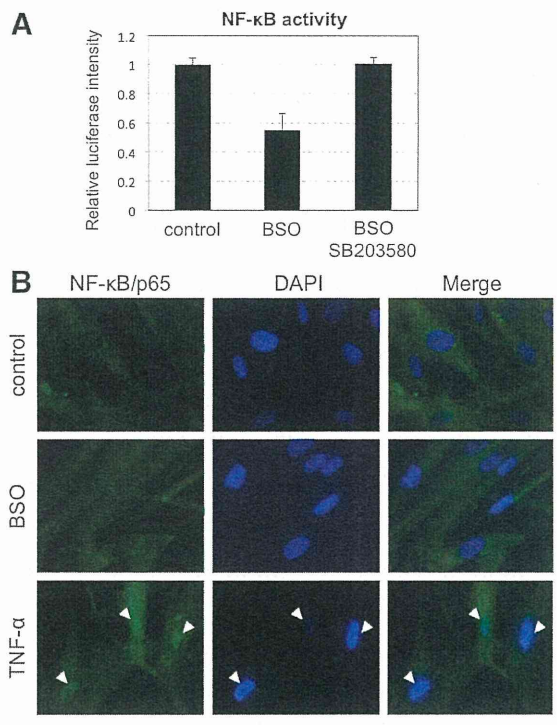

Figure 6 Transcriptional activity of NF-κB was not stimulated by oxidative stress. hADMPCs were transfected with pNF-κB-Luc and were treated with 10 μM of SB203580 or 0.1% DMSO for 2 h followed by addition of 1 mM of BSO. After 24 h, the medium was changed to fresh medium and cells were cultured for an additional 2 days. **(A)** The activity of NF-κB was measured by the intensity of luciferase activity driven from a minimal promoter containing tandem repeats of the NFκB transcriptional response element. Data shown represent the average of 3 independent experiments. **(B)** Immunocytochemical analysis against NF-κB/p65 (green). Blue staining represents nuclear staining by DAPI. Note that nuclear localization of NF-κB/p65 (white arrowhead) is only observed in hADMPCs treated with 20 ng/mL of TNF-α.

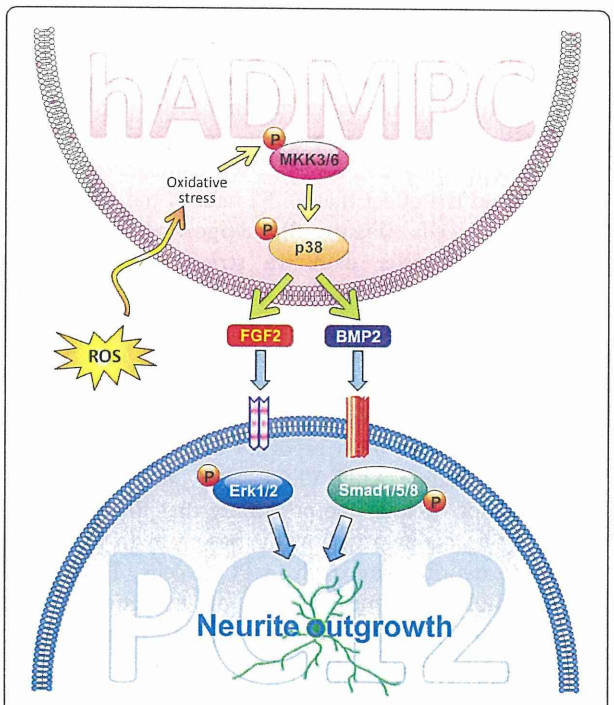

Figure 7 Model of this study. A schematic illustration of the results of this study is shown. Oxidative stress by BSO treatment in hADMPCs results in p38 MAPK activation, which then leads to BMP2 and FGF2 expression and secretion. The secreted factors then bind to the receptors on PC12 cells, facilitating neural differentiation in these cells.

Discussion

In this study, we investigated the effect of oxidative stress in hADMPCs on the induction of neuronal differentiation. Such mechanisms may explain how administration of hADMPCs to neurodegenerative lesions enhances endogenous repair mechanisms via neurogenesis of endogenous neural progenitor and stem cells. Damaged tissues, such as the brain tissue of patients who have suffered from ischemic stroke, are subject to inflammation and the generation of reactive oxygen species (ROS) [17,18]. Our data demonstrated that hADMPCs, when exposed to oxidative stress, facilitate neuronal differentiation in rat pheochromocytoma cell line PC12 cells by upregulation of fibroblast growth factor 2 (FGF2) and bone morphogenetic protein 2 (BMP2) secretion through p38 MAPK activation.

Our results show that BMP2 and FGF2 were upregulated in hADMPCs when exposed to buthionine sulfoximine (BSO), a glutathione-synthesis inhibitor that leads to oxidative stress. These findings may have therapeutic implications in neurodegenerative diseases. We concluded that BMP2 and FGF2 secreted from hADMPCs that had been exposed to oxidative stress were the main inducers of neurite outgrowth in PC12 cells. Erk1/2 and

Smad1/5/8 were significantly activated in these cells (Figure 2), while other growth factors known to induce neurite outgrowth in PC12 cells such as nerve growth factor (NGF) and vascular endothelial growth factor (VEGF) were not observed to be upregulated by BSO treatment (data not shown). We confirmed that BMP2 enhanced the effect that FGF2 had on the differentiation of PC12 cells (Figure 3), supporting our idea that hADMPCs under oxidative stress conditions secrete BMP2 and FGF2 and that this contributes to neuronal differentiation. Consistent with our conclusions, it has been reported that BMP2, via activation of a Smad signaling pathway, facilitated FGF2-induced neuronal differentiation in PC12 cells [26,27]. However, since hADMPCs have been reported to secrete many growth factor including NGF, VEGF, HGF, and IGF [11,15,33], we cannot exclude the possibility that BMP2 and FGF2 are acting cooperatively with these growth factors to facilitate neurite outgrowth in PC12 cells. Thus, the precise molecular mechanisms of induction of PC12 differentiation and the precise expression profiles in BSO-treated hADMPCs need to be further investigated.

Recently, BMP signaling through Smad1/5/8 has been reported to contribute to neurite outgrowth in dorsal root ganglion neurons both in vitro and in vivo [34,35]. Moreover, BMP2 has been shown to have neurotrophic effects on midbrain dopaminergic neurons [36], ventral mesencephalic neurons [37], mouse embryonic striatal neurons [38], and nitrergic and catecholaminergic enteric neurons [39]. Moreover, FGF2 is trophic for neurons, glias, and endothelial cells in the central nervous system. FGF2 also prevents downregulation of the anti-apoptotic protein Bcl-2 in ischemic brain tissue and limits its excitotoxic damage to the brain through an activin-dependent mechanism [40]. These findings are consistent with our hypothesis that hADMPCs secret BMP2 and FGF2 to induce neurogenesis in neurodegenerative lesions in response to oxidative stress.

As it has been shown that ROS activate ERKs, JNKs, and p38 MAPKs [28,29], we examined the MAPK signaling pathway in hADMPCs exposed to oxidative stress and found that BSO treatment resulted in significant activation of ERK1/2 and p38 MAPK. Intriguingly, addition of SB203580, a specific inhibitor of p38 MAPK, but not the ERK inhibitor U0126, suppressed *BMP2* and *FGF2* expression in BSO-treated hADMPCs to control levels (Figure 4), suggesting that p38 MAPK was contributing to upregulation of BMP2 and FGF2 in hADMPCs when exposed to oxidative stress. Moreover, lentiviral transduction of the constitutively active form of MKK6, a MAPKK that selectively activates p38 MAPK isoforms [30], resulted in upregulation of BMP2 and FGF2 and this also demonstrated the crucial role of the p38 MAPK cascade in the regulation of BMP2 and FGF2. In primary human endothelial cells, p38-dependent regulation of BMP2 expression was reported previously. Viemann *et al.* [41] investigated the genes that were induced by inflammatory stimulation with tumor necrosis factor α (TNF-α) and classified these genes into 2 categories based on whether they were regulated in an NF-κB-dependent or p38 MAPK-dependent manner. Consistent with our findings, they found that significant induction of BMP2 expression by TNF-α was markedly suppressed by SB202190, an inhibitor of p38 MAPK. These results support the hypothesis that activation of the p38 MAPK pathway in hADMPCs in response to inflammation surrounding neurodegenerative lesions leads to induction of BMP2 and FGF2, which in turn support regeneration of neuronal cells.

It has been known that NF-κB directly binds to the BMP2 promoter to induce its expression [31], and MSK1, a downstream molecule of p38 MAPK, is involved in NF-κB transactivation [32]. However, we did not observe an elevation of NF-κB transcriptional activity in hADMPCs when they were exposed to oxidative stress (Figure 6). The mechanism of p38-dependent regulation of gene expression is not completely understood, and the precise mechanism by which p38 MAPK regulates the expression of BMP2 and FGF2 remains to be determined.

In this study, we also found that suppression of ERK1/2 MAPK by U0126 in BSO-treated hADMPCs resulted in slight activation of p38 MAPK (Figure 4A). Consistent with this, the expression level of *BMP2* mRNA was also upregulated when cells exposed to oxidative stress were pretreated with U0126 (Figure 4C). Previously, "seesaw cross-talk" between ERK and p38 MAPK signaling has been reported; i.e., the MEK inhibitor caused a decrease in the phosphorylation level of ERK and an increase in that of p38, whereas the p38 inhibitor had the opposite effect [42-44]. We did not investigate the phosphorylation of ERK1/2 in SB203580-treated hADMPCs, but it may be possible that seesaw cross-talk also occurs in our system.

Conclusions

In summary, the results obtained in this study have demonstrated the potential use of hADMPCs for the treatment of neurodegenerative diseases such as ischemic stroke, Parkinson's disease, Alzheimer's disease, and spinal cord injury, in which the transplanted hADMPCs might be exposed to oxidative stress. Moreover, the p38-dependent modulation of BMP2 and FGF2 expression observed in this study is expected to be a new therapeutic target for neurodegenerative disorders.

Materials and methods

Adipose tissue samples

Subcutaneous adipose tissue samples (10–50 g, each) were resected during plastic surgery in 5 females (age,

20–60 years) as excess discards. The study protocol was approved by the Review Board for Human Research of Kobe University Graduate School of Medicine, Foundation for Biomedical Research and Innovation and Kinki University Pharmaceutical Research and Technology Institute (reference number: 10–005). Each subject provided a signed informed consent.

Cell culture

PC12 cells were obtained from the Health Science Research Resources Bank (Osaka, Japan) and maintained in RPMI1640 media supplemented with 10% heat-inactivated horse serum and 5% fetal bovine serum. For differentiation, the cells were plated in 6-well culture plates coated with collagen type I (Nitta Gelatin, Osaka, Japan) and the medium was replaced with differentiation medium (RPMI1640 supplemented with 1% horse serum and 0.5% fetal bovine serum) or conditioned medium from hADMPCs. NGF (50 ng/mL), BMP2 (40 ng/mL) or FGF2 (5 ng/mL) were added to the differentiation medium. Recombinant murine Noggin (200 ng/mL: PeproTech, NJ, USA) was added to conditioned medium from BSO-treated hADMPCs. hADMPCs were isolated as previously reported [4-6,45,46] and maintained in a medium containing 60% DMEM-low glucose, 40% MCDB-201 medium (Sigma Aldrich, St. Louis, MO, USA), 1× insulin-transferrin-selenium (Gibco Invitrogen, NY, USA), 1 nM dexamethasone (Sigma Aldrich), 100 mM ascorbic acid 2-phosphate (Wako, Osaka, Japan), 10 ng/mL epidermal growth factor (PeproTech), and 5% fetal bovine serum. The cells were plated to a density of 5×10^3 cells/cm^2 on fibronectin-coated dishes, and the medium was replaced every 2 days.

Preparation of conditioned medium from hADMPCs

Two days after plating, hADMPCs were treated with BSO (concentrations used were varied in each experiment and are indicated in the results and figure legends) for 16 h. The medium was replaced with fresh culture medium for 2 days followed by replacement with PC12 cell differentiation medium. After 2 more days, the medium was removed for use as conditioned medium. For preparation of the conditioned medium from hADMPCs in which one of the three, p38, Erk1/2, or JNK MAPK, was inhibited, hADMPCs were pretreated with 10 μM SB203580 (Promega, WI, USA), 10 μM U0126 (Promega), or 10 μM JNK inhibitor II (EMD4 Bioscience, CA, USA), respectively, for 2 h and subsequently treated with 1 mM BSO.

Measurement of GSH/GSSG ratio

Ratios of reduced glutathione (GSH) to oxidized glutathione (GSSG) were measured using the GSH/GSSG-Glo assay kit (Promega) following the manufacturer's protocol.

Measurement of reactive oxygen species production

Cells were harvested and incubated with 10 μM 5-(and-6)-chloromethyl-2',7'-dichlorodihydrofluorescein diacetate, acetyl ester (CM-H_2DCFDA). The amount of intracellular ROS production was proportional to green fluorescence, as analyzed with a Guava easyCyte 8HT flow cytometer (Millipore) using an argon laser at 488 nm and a 525/30 nm band pass filter, and dead cells were excluded with the LIVE/DEAD fixable far red dead cell stain kit (Invitrogen).

Western blot analysis

Cells were washed with ice-cold phosphate-buffered saline and lysed with M-PER Mammalian Protein Extraction Reagent (Thermo Scientific Pierce, IL, USA) following the manufacturer's instructions. Equal amounts of proteins were separated by sodium dodecylsulfate polyacrylamide gel electrophoresis (SDS-PAGE), transferred to polyvinylidene fluoride (PVDF) membranes (Immobilon-P; Millipore, MA, USA), and probed with antibodies against phospho-Erk1/2 (#4370), Erk1/2 (#4695), phospho-38 (#9215), p38 (#9212), phospho-Smad1/5/8 (#9511), phospho-Akt (#4060), Akt (#4691), phospho-JNK (#9251), JNK (#9258) (all from Cell Signaling Technology, MA, USA) and actin (Millipore). Horseradish peroxidase (HRP)-conjugated anti-rabbit and anti-mouse secondary antibodies (Cell Signaling Technology, Danvers, MA, USA) were used as probes and immunoreactive bands were visualized with the Immobilon Western Chemiluminescent HRP substrate (Millipore). The band intensity was measured using ImageJ software.

RNA extraction, cDNA generation, and quantitative polymerase chain reaction (q-PCR)

Total RNA was extracted using the RNeasy Mini Kit (Qiagen, Hilden, Germany) following the manufacturer's instructions. cDNA was generated from 1 μg of total RNA using the Verso cDNA Synthesis Kit (Thermo Scientific) and purified with the MinElute PCR Purification Kit (Qiagen). Q-PCR analysis was carried out using the SsoFast EvaGreen supermix (Bio-Rad, CA, USA) according to the manufacturer's protocols. The relative expression value of each gene was calculated using a ΔΔCt method and the most reliable internal control gene was determined using the geNorm Software (http://medgen.ugent.be/~jvdesomp/genorm/). Details of the primers used in these experiments are available on request.

Enzyme-linked immunosorbent assay

Enzyme-linked immunosorbent assay (ELISA) was performed using the Quantikine BMP-2 Immunoassay System and Quantikine FGF-2 Immunoassay System (R&D

Systems, MN, USA) following the manufacturer's protocols.

Plasmid construction and lentivirus production

Flag-tagged MKK6 (glu) [30] was provided by Addgene (pcDNA3-Flag MKK6 (glu); Addgene plasmid 13518). Flag-tagged MKK6 (glu) was cloned into a pENTR11 vector (Invitrogen). An iresGFP fragment was subsequently cloned into the plasmid to produce the entry vector pENTR11-MKK6 (glu)-iresGFP. The entry vector and CSII-EF-RfA (kindly provided by Dr. Miyoshi, RIKEN BioResource Center, Tsukuba, Japan) were incubated with LR clonase II enzyme mix (Invitrogen) to generate CSII-EF-MKK6 (glu)-iresGFP. The resultant plasmid was mixed with packaging plasmids (pCAG-HIVg/p and pCMV-VSVG-RSV-Rev, kindly provided by Dr. Miyoshi) and transfected into 293 T cells. The supernatant medium, which contained lentiviral vectors, was collected 2 days after transduction and concentrated by centrifugation (6000 G, 15 h, 4°C).

Luciferase assay

hADMPCs were transfected with pGL4.74 (Promega) and either pTAL-Luc or pNF-κB-Luc by TransIT-2020 (TaKaRa-Bio). The cells were then treated with 10 μM of SB203580 or 0.1% DMSO for 2 h followed by addition of 1 mM of BSO. After 24 h, the medium was changed to fresh medium and cells were cultured for an additional 2 days. The activity of NF-κB was measured using the Dual Luciferases Assay System (Promega) according to the manufacturer's protocol.

Immunocytochemistry

hADMPCs were fixed with 4% paraformaldehyde in PBS for 10 min at 4°C and then washed 3 times in PBS. Blocking was performed with PBSMT (PBS containing 0.1% Triton X-100, 2% Skim Milk) for 1 h at room temperature. The cells were then incubated with rabbit monoclonal antibody against NF-κB p65 (Cell Signaling; #8242; 1/100 dilution) overnight at 4°C. After washing with PBS, cells were incubated with Alexa 488 conjugated anti-rabbit IgG (Invitrogen; 1/1000 dilution) for 1 h. The cells were counterstained with 4′-6-diamidino-2-phenylindole (DAPI) (Invitrogen) to identify cellular nuclei.

Competing interests

None of the authors have any competing interests related to the manuscript.

Authors' contributions

MM carried out the FACS analysis, qPCR analysis, ELISA, immunofluorescent staining, and cell culture, participated in the study design, and drafted the manuscript. HM participated in the study design, carried out the western blot analysis, luciferase assay, and cell culture, and drafted the manuscript. AU carried out western blot analysis, constructed the plasmids, and generated the lentiviral vectors. YN carried out qPCR analysis and performed the statistical analysis. AI resected subcutaneous adipose tissue samples during plastic surgery. HO and AM isolated hADMPCs from human adipose tissues. TH conceived the study, participated in its design and coordination, and helped to draft the manuscript. All authors read and approved the final manuscript.

Acknowledgements

We thank A Nishikawa, T Fukase, T Sasaki, T Shoji, K Nakagita, S Fukui, and K Honjo for technical support. We thank Dr. Roger Davis for providing the pcDNA3-Flag MKK6 (glu) plasmid and Dr. Hiroyuki Miyoshi for the CSII-EF-RfA, pCMV-VSVG-RSV-Rev and pCMV-HIVg/p plasmids. This work was supported in part by grants from the Ministry of Health, Labor, and Welfare of Japan and a grant from the Program for Promotion of Fundamental Studies in Health Sciences of the National Institute of Biomedical Innovation (NIBIO).

Author details

[1]Pharmaceutical Research and Technology Institute, Kinki University, 3-4-1 Kowakae, Higashi-Osaka, Osaka 577-8502, Japan. [2]Department of Somatic Stem Cell Therapy and Health Policy, Foundation for Biomedical Research and Innovation, TRI305, 1-5-4 Minatojima-minamimachi, Chuo-ku, Kobe, Hyogo 650-0047, Japan. [3]Department of Plastic Surgery, Kobe University Hospital, Kobe, Japan.

Received: 28 March 2012 Accepted: 2 August 2012
Published: 7 August 2012

References

1. Pittenger MF, Mackay AM, Beck SC, Jaiswal RK, Douglas R, Mosca JD, Moorman MA, Simonetti DW, Craig S, Marshak DR: **Multilineage potential of adult human mesenchymal stem cells.** *Science* 1999, **284**:143–147.
2. Bieback K, Kern S, Kluter H, Eichler H: **Critical parameters for the isolation of mesenchymal stem cells from umbilical cord blood.** *Stem Cells* 2004, **22**:625–634.
3. Zuk PA, Zhu M, Ashjian P, De Ugarte DA, Huang JI, Mizuno H, Alfonso ZC, Fraser JK, Benhaim P, Hedrick MH: **Human adipose tissue is a source of multipotent stem cells.** *Mol Biol Cell* 2002, **13**:4279–4295.
4. Okura H, Komoda H, Saga A, Kakuta-Yamamoto A, Hamada Y, Fumimoto Y, Lee CM, Ichinose A, Sawa Y, Matsuyama A: **Properties of hepatocyte-like cell clusters from human adipose tissue-derived mesenchymal stem cells.** *Tissue Eng Part C Methods* 2010, **16**:761–770.
5. Okura H, Matsuyama A, Lee CM, Saga A, Kakuta-Yamamoto A, Nagao A, Sougawa N, Sekiya N, Takekita K, Shudo Y, *et al*: **Cardiomyoblast-like cells differentiated from human adipose tissue-derived mesenchymal stem cells improve left ventricular dysfunction and survival in a rat myocardial infarction model.** *Tissue Eng Part C Methods* 2010, **16**:417–425.
6. Komoda H, Okura H, Lee CM, Sougawa N, Iwayama T, Hashikawa T, Saga A, Yamamoto-Kakuta A, Ichinose A, Murakami S, Sawa Y, Matsuyama A: **Reduction of N-glycolylneuraminic acid xenoantigen on human adipose tissue-derived stromal cells/mesenchymal stem cells leads to safer and more useful cell sources for various stem cell therapies.** *Tissue Eng Part A* 2010, **16**:1143–1155.
7. Okura H, Komoda H, Fumimoto Y, Lee CM, Nishida T, Sawa Y, Matsuyama A: **Transdifferentiation of human adipose tissue-derived stromal cells into insulin-producing clusters.** *J Artif Organs* 2009, **12**:123–130.
8. Safford KM, Safford SD, Gimble JM, Shetty AK, Rice HE: **Characterization of neuronal/glial differentiation of murine adipose-derived adult stromal cells.** *Exp Neurol* 2004, **187**:319–328.
9. Leu S, Lin YC, Yuen CM, Yen CH, Kao YH, Sun CK, Yip HK: **Adipose-derived mesenchymal stem cells markedly attenuate brain infarct size and improve neurological function in rats.** *J Transl Med* 2010, **8**:63.
10. Ikegame Y, Yamashita K, Hayashi S, Mizuno H, Tawada M, You F, Yamada K, Tanaka Y, Egashira Y, Nakashima S, Yoshimura S, Iwama T: **Comparison of mesenchymal stem cells from adipose tissue and bone marrow for ischemic stroke therapy.** *Cytotherapy* 2011, **13**:675–685.
11. Tan B, Luan Z, Wei X, He Y, Wei G, Johnstone BH, Farlow M, Du Y: **AMP-activated kinase mediates adipose stem cell-stimulated neuritogenesis of PC12 cells.** *Neuroscience* 2011, **181**:40–47.
12. Reid AJ, Sun M, Wiberg M, Downes S: *Terenghi G.* Kingham PJ: Nerve repair with adipose-derived stem cells protects dorsal root ganglia neurons from apoptosis. Neuroscience; 2011.

13. Rehman J, Traktuev D, Li J, Merfeld-Clauss S, Temm-Grove CJ, Bovenkerk JE, Pell CL, Johnstone BH, Considine RV, March KL: **Secretion of angiogenic and antiapoptotic factors by human adipose stromal cells.** *Circulation* 2004, **109**:1292–1298.
14. Lee EY, Xia Y, Kim WS, Kim MH, Kim TH, Kim KJ, Park BS, Sung JH: **Hypoxia-enhanced wound-healing function of adipose-derived stem cells: increase in stem cell proliferation and up-regulation of VEGF and bFGF.** *Wound Repair Regen* 2009, **17**:540–547.
15. Lu S, Lu C, Han Q, Li J, Du Z, Liao L, Zhao RC: **Adipose-derived mesenchymal stem cells protect PC12 cells from glutamate excitotoxicity-induced apoptosis by upregulation of XIAP through PI3-K/Akt activation.** *Toxicology* 2011, **279**:189–195.
16. McCoy MK, Martinez TN, Ruhn KA, Wrage PC, Keefer EW, Botterman BR, Tansey KE, Tansey MG: **Autologous transplants of Adipose-Derived Adult Stromal (ADAS) cells afford dopaminergic neuroprotection in a model of Parkinson's disease.** *Exp Neurol* 2008, **210**:14–29.
17. Flamm ES, Demopoulos HB, Seligman ML, Poser RG, Ransohoff J: **Free radicals in cerebral ischemia.** *Stroke* 1978, **9**:445–447.
18. Alexandrova ML, Bochev PG: **Oxidative stress during the chronic phase after stroke.** *Free Radic Biol Med* 2005, **39**:297–316.
19. Lambeth JD: **NOX enzymes and the biology of reactive oxygen.** *Nat Rev Immunol* 2004, **4**:181–189.
20. Simpson JE, Ince PG, Haynes LJ, Theaker R, Gelsthorpe C, Baxter L, Forster G, Lace GL, Shaw PJ, Matthews FE, Savva GM, Brayne C, Wharton SB, MRC Cognitive Function and Ageing Neuropathology Study Group: **Population variation in oxidative stress and astrocyte DNA damage in relation to Alzheimer-type pathology in the ageing brain.** *Neuropathol Appl Neurobiol* 2010, **36**:25–40.
21. Cai Z, Zhao B, Ratka A: **Oxidative Stress and beta-Amyloid Protein in Alzheimer's Disease.** *Neuromolecular Med* 2011, **13**:223–250.
22. Beal MF: **Mitochondria, oxidative damage, and inflammation in Parkinson's disease.** *Ann N Y Acad Sci* 2003, **991**:120–131.
23. Henchcliffe C, Beal MF: **Mitochondrial biology and oxidative stress in Parkinson disease pathogenesis.** *Nat Clin Pract Neurol* 2008, **4**:600–609.
24. Minghetti L, Ajmone-Cat MA, De Berardinis MA, De Simone R: **Microglial activation in chronic neurodegenerative diseases: roles of apoptotic neurons and chronic stimulation.** *Brain Res Brain Res Rev* 2005, **48**:251–256.
25. Colton CA, Chernyshev ON, Gilbert DL, Vitek MP: **Microglial contribution to oxidative stress in Alzheimer's disease.** *Ann N Y Acad Sci* 2000, **899**:292–307.
26. Hayashi H, Ishisaki A, Suzuki M, Imamura T: **BMP-2 augments FGF-induced differentiation of PC12 cells through upregulation of FGF receptor-1 expression.** *J Cell Sci* 2001, **114**:1387–1395.
27. Hayashi H, Ishisaki A, Imamura T: **Smad mediates BMP-2-induced upregulation of FGF-evoked PC12 cell differentiation.** *FEBS Lett* 2003, **536**:30–34.
28. Son Y, Cheong YK, Kim NH, Chung HT, Kang DG, Pae HO: **Mitogen-Activated Protein Kinases and Reactive Oxygen Species: How Can ROS Activate MAPK Pathways?** *J Signal Transduct* 2011, **2011**:792639.
29. Ito K, Hirao A, Arai F, Takubo K, Matsuoka S, Miyamoto K, Ohmura M, Naka K, Hosokawa K, Ikeda Y, Suda T: **Reactive oxygen species act through p38 MAPK to limit the lifespan of hematopoietic stem cells.** *Nat Med* 2006, **12**:446–451.
30. Raingeaud J, Whitmarsh AJ, Barrett T, Derijard B, Davis RJ: **MKK3- and MKK6-regulated gene expression is mediated by the p38 mitogen-activated protein kinase signal transduction pathway.** *Mol Cell Biol* 1996, **16**:1247–1255.
31. Feng JQ, Xing L, Zhang JH, Zhao M, Horn D, Chan J, Boyce BF, Harris SE, Mundy GR, Chen D: **NF-kappaB specifically activates BMP-2 gene expression in growth plate chondrocytes in vivo and in a chondrocyte cell line in vitro.** *J Biol Chem* 2003, **278**:29130–29135.
32. Vermeulen L, De Wilde G, Van Damme P: **Vanden Berghe W, Haegeman G: Transcriptional activation of the NF-kappaB p65 subunit by mitogen- and stress-activated protein kinase-1 (MSK1).** *EMBO J* 2003, **22**:1313–1324.
33. Rasmussen JG, Frobert O, Pilgaard L, Kastrup J, Simonsen U, Zachar V, Fink T: **Prolonged hypoxic culture and trypsinization increase the pro-angiogenic potential of human adipose tissue-derived stem cells.** *Cytotherapy* 2011, **13**:318–328.
34. Parikh P, Hao Y, Hosseinkhani M, Patil SB, Huntley GW, Tessier-Lavigne M, Zou H: **Regeneration of axons in injured spinal cord by activation of bone morphogenetic protein/Smad1 signaling pathway in adult neurons.** *Proc Natl Acad Sci U S A* 2011, **108**:E99–E107.
35. Ma CH, Brenner GJ, Omura T, Samad OA, Costigan M, Inquimbert P, Niederkofler V, Salie R, Sun CC, Lin HY, Arber S, Coppola G, Woolf CJ, Samad TA: **The BMP coreceptor RGMb promotes while the endogenous BMP antagonist noggin reduces neurite outgrowth and peripheral nerve regeneration by modulating BMP signaling.** *J Neurosci* 2011, **31**:18391–18400.
36. Jordan J, Bottner M, Schluesener HJ, Unsicker K, Krieglstein K: **Bone morphogenetic proteins: neurotrophic roles for midbrain dopaminergic neurons and implications of astroglial cells.** *Eur J Neurosci* 1997, **9**:1699–1709.
37. Reiriz J, Espejo M, Ventura F, Ambrosio S, Alberch J: **Bone morphogenetic protein-2 promotes dissociated effects on the number and differentiation of cultured ventral mesencephalic dopaminergic neurons.** *J Neurobiol* 1999, **38**:161–170.
38. Stull ND, Jung JW, Iacovitti L: **Induction of a dopaminergic phenotype in cultured striatal neurons by bone morphogenetic proteins.** *Brain Res Dev Brain Res* 2001, **130**:91–98.
39. Anitha M, Shahnavaz N, Qayed E, Joseph I, Gossrau G, Mwangi S, Sitaraman SV, Greene JG, Srinivasan S: **BMP2 promotes differentiation of nitrergic and catecholaminergic enteric neurons through a Smad1-dependent pathway.** *Am J Physiol Gastrointest Liver Physiol* 2010, **298**:G375–G383.
40. Ikeda N, Nonoguchi N, Zhao MZ, Watanabe T, Kajimoto Y, Furutama D, Kimura F, Dezawa M, Coffin RS, Otsuki Y, Kuroiwa T, Miyatake S: **Bone marrow stromal cells that enhanced fibroblast growth factor-2 secretion by herpes simplex virus vector improve neurological outcome after transient focal cerebral ischemia in rats.** *Stroke* 2005, **36**:2725–2730.
41. Viemann D, Goebeler M, Schmid S, Klimmek K, Sorg C, Ludwig S, Roth J: **Transcriptional profiling of IKK2/NF-kappa B- and p38 MAP kinase-dependent gene expression in TNF-alpha-stimulated primary human endothelial cells.** *Blood* 2004, **103**:3365–3373.
42. Hotokezaka H, Sakai E, Kanaoka K, Saito K, Matsuo K, Kitaura H, Yoshida N, Nakayama K: **U0126 and PD98059, specific inhibitors of MEK, accelerate differentiation of RAW264.7 cells into osteoclast-like cells.** *J Biol Chem* 2002, **277**:47366–47372.
43. Shimo T, Matsumura S, Ibaragi S, Isowa S, Kishimoto K, Mese H, Nishiyama A, Sasaki A: **Specific inhibitor of MEK-mediated cross-talk between ERK and p38 MAPK during differentiation of human osteosarcoma cells.** *J Cell Commun Signal* 2007, **1**:103–111.
44. Al-Shanti N, Stewart CE: **PD98059 enhances C2 myoblast differentiation through p38 MAPK activation: a novel role for PD98059.** *J Endocrinol* 2008, **198**:243–252.
45. Okura H, Saga A, Fumimoto Y, Soeda M, Moriyama M, Moriyama H, Nagai K, Lee CM, Yamashita S, Ichinose A, Hayakawa T, Matsuyama A: **Transplantation of human adipose tissue-derived multilineage progenitor cells reduces serum cholesterol in hyperlipidemic Watanabe rabbits.** *Tissue Eng Part C Methods* 2011, **17**:145–154.
46. Saga A, Okura H, Soeda M, Tani J, Fumimoto Y, Komoda H, Moriyama M, Moriyama H, Yamashita S, Ichinose A, Daimon T, Hayakawa T, Matsuyama A: **HMG-CoA reductase inhibitor augments the serum total cholesterol-lowering effect of human adipose tissue-derived multilineage progenitor cells in hyperlipidemic homozygous Watanabe rabbits.** *Biochem Biophys Res Commun* 2011, **412**:50–54.

doi:10.1186/1471-2121-13-21
Cite this article as: Moriyama *et al.*: Human adipose tissue-derived multilineage progenitor cells exposed to oxidative stress induce neurite outgrowth in PC12 cells through p38 MAPK signaling. *BMC Cell Biology* 2012 **13**:21.

Biomaterials 34 (2013) 1781–1789

Contents lists available at SciVerse ScienceDirect

Biomaterials

journal homepage: www.elsevier.com/locate/biomaterials

3D spheroid culture of hESC/hiPSC-derived hepatocyte-like cells for drug toxicity testing

Kazuo Takayama [a,b], Kenji Kawabata [b,c], Yasuhito Nagamoto [a,b], Keisuke Kishimoto [a,b], Katsuhisa Tashiro [b], Fuminori Sakurai [a], Masashi Tachibana [a], Katsuhiro Kanda [d], Takao Hayakawa [e], Miho Kusuda Furue [f,g], Hiroyuki Mizuguchi [a,b,h,*]

[a] Laboratory of Biochemistry and Molecular Biology, Graduate School of Pharmaceutical Sciences, Osaka University, Osaka 565-0871, Japan
[b] Laboratory of Stem Cell Regulation, National Institute of Biomedical Innovation, Osaka 567-0085, Japan
[c] Laboratory of Biomedical Innovation, Graduate School of Pharmaceutical Sciences, Osaka University, Osaka 565-0871, Japan
[d] Pharma Business Project, Corporate Projects Center, Corporate Strategy Division, Hitachi High-Technologies Corporation, Ibaraki 312-8504, Japan
[e] Pharmaceutical Research and Technology Institute, Kinki University, Osaka 577-8502, Japan
[f] Laboratory of Embryonic Stem Cell Cultures, Department of Disease Bioresources Research, National Institute of Biomedical Innovation, Osaka 567-0085, Japan
[g] Department of Embryonic Stem Cell Research, Field of Stem Cell Reseach, Institute for Frontier Medical Sciences, Kyoto University, Kyoto 606-8507, Japan
[h] The Center for Advanced Medical Engineering and Informatics, Osaka University, Osaka 565-0871, Japan

ARTICLE INFO

Article history:
Received 11 September 2012
Accepted 20 November 2012
Available online 8 December 2012

Keywords:
Hepatocyte-like cell
Human ES cell
Human iPS cell
Nanopillar plate
Drug screening

ABSTRACT

Although it is expected that hepatocyte-like cells differentiated from human embryonic stem (ES) cells or induced pluripotent stem (iPS) cells will be utilized in drug toxicity testing, the actual applicability of hepatocyte-like cells in this context has not been well examined so far. To generate mature hepatocyte-like cells that would be applicable for drug toxicity testing, we established a hepatocyte differentiation method that employs not only stage-specific transient overexpression of hepatocyte-related transcription factors but also a three-dimensional spheroid culture system using a Nanopillar Plate. We succeeded in establishing protocol that could generate more matured hepatocyte-like cells than our previous protocol. In addition, our hepatocyte-like cells could sensitively predict drug-induced hepatotoxicity, including reactive metabolite-mediated toxicity. In conclusion, our hepatocyte-like cells differentiated from human ES cells or iPS cells have potential to be applied in drug toxicity testing.

1. Introduction

Hepatocyte-like cells that are generated from human embryonic stem cells (hESCs) [1] or human induced pluripotent stem cells (hiPSCs) [2] are expected to be used in drug screening instead of primary (or cryopreserved) human hepatocytes (PHs). We recently demonstrated that stage-specific transient transduction of transcription factors, in addition to treatment with optimal growth factors and cytokines, is useful for promoting hepatic differentiation [3–6]. The hepatocyte-like cells, which have many hepatocyte characteristics (the abilities to uptake low-density lipoprotein and Indocyanine green, store glycogen, and synthesize urea) and drug metabolism capacity, were generated from hESCs/hiPSCs by combinational transduction of FOXA2 and HNF1α [6]. However, further maturation of the hepatocyte-like cells is required because their hepatic characteristics, such as drug metabolism capacity, are lower than those of PHs [6].

To promote further maturation of the hepatocyte-like cells, we subjected them to three-dimensional (3D) spheroid cultures. It is known that various 3D culture conditions (such as Algimatrix scaffolds [7], cell sheet technology [8], galactose-carrying substrata [9], and basement membrane substratum [10]) are useful for the maturation of the hepatocyte-like cells. Nanopillar Plate technology [11] used in the present study makes it easy to control the configuration of the spheroids. The Nanopillar Plate has an arrayed μm-scale hole structure at the bottom of each well, and nanopillars were aligned further at the bottom of the respective holes. The seeded cells evenly drop into the holes, then migrate and aggregate on top surface of the nanopillars, thus likely to form the uniform spheroids in each hole. Not only 3D spheroid cultures [12] but also Matrigel overlay cultures [13] are useful for maintaining the hepatocyte characteristics of PHs. Therefore, we employed both 3D

* Corresponding author. Laboratory of Biochemistry and Molecular Biology, Graduate School of Pharmaceutical Sciences, Osaka University, 1-6 Yamadaoka, Suita, Osaka 565-0871, Japan. Tel.: +81 6 6879 8185; fax: +81 6 6879 8186.
E-mail address: mizuguch@phs.osaka-u.ac.jp (H. Mizuguchi).

0142-9612/$ – see front matter © 2012 Elsevier Ltd. All rights reserved.
http://dx.doi.org/10.1016/j.biomaterials.2012.11.029

spheroid culture and Matrigel overlay culture systems to promote hepatocyte maturation of the hepatocyte-like cells.

The hepatocyte-like cells generated from hESCs/hiPSCs are expected to be used in drug development. To the best of our knowledge, however, few studies have tried to predict widespread drug-induced cytotoxicity *in vitro* using the hepatocyte-like cells. To precisely determine the applicability of the hepatocyte-like cells to drug screening, it is necessary to investigate the responses of these hepatocyte-like cells to many kinds of hepatotoxic drugs.

In this study, 3D spheroid and Matrigel overlay cultures of the hepatocyte-like cells were performed to promote hepatocyte maturation. The gene expression analysis of cytochrome P450 (CYP) enzymes, conjugating enzymes, hepatic transporters, and hepatic nuclear receptors in the 3D spheroid-cultured hESC- or hiPSC-derived hepatocyte-like cells (3D ES-hepa or 3D iPS-hepa), were analyzed. In addition, CYP induction potency and drug metabolism capacity were estimated in the 3D ES/iPS-hepa. To determine the suitability of these cells for drug screening, we examined whether the drug-induced cytotoxicity is induced by treatment of various kinds of hepatotoxic drugs in 3D ES/iPS-hepa.

2. Materials and methods

2.1. hESCs and hiPSCs culture

A hESC line, H1 and H9 (WiCell Research Institute), was maintained on a feeder layer of mitomycin C-treated mouse embryonic fibroblasts (Millipore) with Repro Stem medium (Repro CELL) supplemented with 5 ng/ml fibroblast growth factor 2 (FGF2) (Sigma). Both H1 and H9 were used following the Guidelines for Derivation and Utilization of Human Embryonic Stem Cells of the Ministry of Education, Culture, Sports, Science and Technology of Japan and furthermore, and the study was approved by Independent Ethics Committee.

Three human iPSC lines were provided from the JCRB Cell Bank (Tic, JCRB Number: JCRB1331; Dotcom, JCRB Number: JCRB1327; Toe, JCRB Number: JCRB1338) [14,15]. These human iPSC lines were maintained on a feeder layer of mitomycin C-treated mouse embryonic fibroblasts with iPSellon (Cardio) supplemented with 10 ng/ml FGF2. Other three human iPSC lines, 201B6, 201B7 and 253G1 were kindly provided by Dr. S. Yamanaka (Kyoto University) [2]. These human iPSC lines were maintained on a feeder layer of mitomycin C-treated mouse embryonic fibroblasts with Repro Stem supplemented with 5 ng/ml FGF2.

2.2. In vitro differentiation

Before the initiation of cellular differentiation, the medium of hESCs was exchanged into a defined serum-free medium, hESF9, and cultured as previously reported [16]. The differentiation protocol for the induction of definitive endoderm cells, hepatoblasts, and hepatocytes was based on our previous reports with some modifications [3–5,17]. Briefly, in mesendoderm differentiation, hESCs were dissociated into single cells by using Accutase (Millipore) and cultured for 2 days on Matrigel (BD Biosciences) in differentiation hESF-DIF medium which contains 100 ng/ml Activin A (R&D Systems) and 10 ng/ml bFGF (hESF-DIF medium was purchased from Cell Science & Technology Institute; differentiation hESF-DIF medium was supplemented with 10 μg/ml human recombinant insulin, 5 μg/ml human apotransferrin, 10 μM 2-mercaptoethanol, 10 μM ethanolamine, 10 μM sodium selenite, and 0.5 mg/ml bovine fatty acid free serum albumin [all from sigma]). To generate definitive endoderm cells, the mesendoderm cells were transduced with 3000 vector particle (VP)/cell of Ad-FOXA2 for 1.5 h on day 2 and cultured until day 6 on Matrigel in differentiation hESF-DIF medium supplemented with 100 ng/ml Activin A and 10 ng/ml bFGF. For induction of hepatoblasts, the DE cells were transduced with each 1500 VP/cell of Ad-FOXA2 and Ad-HNF1α for 1.5 h on day 6 and cultured for 3 days on Matrigel in hepatocyte culture medium (HCM) (Lonza) supplemented with 30 ng/ml bone morphogenetic protein 4 (BMP4) (R&D Systems) and 20 ng/ml FGF4 (R&D Systems). In hepatic expansion, the hepatoblasts were transduced with each 1500 VP/cell of Ad-FOXA2 and Ad-HNF1α for 1.5 h on day 9 and cultured for 3 days on Matrigel in HCM supplemented with 10 ng/ml hepatocyte growth factor (HGF), 10 ng/ml FGF1, 10 ng/ml FGF4, and 10 ng/ml FGF10 (all from R&D Systems). To perform hepatocyte maturation on Nanopillar Plate (a prototype multi-well culturing plate for spheroid culture developed and prepared by Hitachi High-Technologies Corporation) shown in Fig. 1B, the cells were seeded at 2.5×10^5 cells/cm^2 (Fig. S1) in hepatocyte culture medium (Fig. S2) supplemented with 10 ng/ml HGF, 10 ng/ml FGF1, 10 ng/ml FGF4, and 10 ng/ml FGF10 on day 11. In the first stage of hepatocyte maturation (from day 12 to day 25), the cells were cultured for 13 days on Matrigel in HCM supplemented with 20 ng/ml HGF, 20 ng/ml oncostatin M (OsM), 10 ng/ml FGF4, and 10^{-6} M dexamethasone (DEX). In the second stage of hepatocyte maturation (from day 25 to day 35), Matrigel was overlaid on the hepatocyte-like cells. Matrigel were diluted to a final concentration of 0.25 mg/ml with William's E medium (Invitrogen) containing 4 mM L-glutamine, 50 ug/ml gentamycin sulfate, 1 × ITS (BD Biosciences), 20 ng/ml OsM, and 10^{-6} M DEX. The culture medium was aspirated, and then the Matrigel solution (described above) was overlaid on the hepatocyte-like cells. The cells were incubated overnight, and the medium was replaced with HCM supplemented with 20 ng/ml OsM and 10^{-6} M DEX.

2.3. Adenovirus (Ad) vectors

Ad vectors were constructed by an improved *in vitro* ligation method [18,19]. The human EF-1α promoter-driven LacZ-, FOXA2-, or HNF1α-expressing Ad vectors (Ad-LacZ, Ad-FOXA2, or Ad-HNF1α, respectively) were constructed previously [3,4,20]. All of Ad vectors contain a stretch of lysine residue (K7) peptides in the C-terminal region of the fiber knob for more efficient transduction of hESCs, hiPSCs, and DE cells, in which transfection efficiency was almost 100%, and purified as described previously [3–5]. The vector particle (VP) titer was determined by using a spectrophotometric method [21].

2.4. Flow cytometry

Single-cell suspensions of hESC/hiPSC-derived cells were fixed with 2% paraformaldehyde (PFA) at 4°C for 20 min, and then incubated with the primary antibody (described in Table S1), followed by the secondary antibody (described in Table S1). Flow cytometry analysis was performed using a FACS LSR Fortessa flow cytometer (BD Biosciences).

2.5. RNA isolation and reverse transcription-polymerase chain reaction (RT-PCR)

Total RNA was isolated from hESCs or hiPSCs and their derivatives using ISOGENE (Nippon Gene). cDNA was synthesized using 500 ng of total RNA with a Superscript VILO cDNA synthesis kit (Invitrogen). Real-time RT-PCR was performed with Taqman gene expression assays (Applied Biosystems) or SYBR Premix Ex Taq (TaKaRa) using an ABI PRISM 7000 Sequence Detector (Applied Biosystems). Relative quantification was performed against a standard curve and the values were normalized against the input determined for the housekeeping gene, glyceraldehyde 3-phosphate dehydrogenase (GAPDH). The primer sequences used in this study are described in Table S2.

2.6. Immunohistochemistry

The cells were fixed with 4% PFA. After incubation with 1% Triton X-100, blocking with Blocking One (Nakalai tesque), the cells were incubated with primary antibody (describe in Table S1) at 4°C for over night, followed by incubation with a secondary antibody (described in Table S1) at room temperature for 1 h.

2.7. ELISA

The hESCs or hiPSCs were differentiated into hepatocytes as described in Fig. 1A. The culture supernatants, which were incubated for 24 h after fresh medium was added, were collected and analyzed for the amount of ALB secretion by ELISA. ELISA kits for ALB were purchased from Bethyl. ELISA was performed according to the manufacturer's instructions. The amount of ALB secretion was calculated according to each standard followed by normalization to the protein content per well.

2.8. Urea secretion

The hESCs or hiPSCs were differentiated into hepatocytes as described in Fig. 1A. The culture supernatants, which were incubated for 24 h after fresh medium was added, were collected and analyzed for the amount of urea secretion. Urea measurement kits were purchased from BioAssay Systems. The experiment was performed according to the manufacturer's instructions. The amount of urea secretion was calculated according to each standard followed by normalization to the protein content per well.

2.9. Canalicular secretory assay

At cellular differentiation, the hepatocyte-like cell spheroids were treated with 5 mM choly-lysyl-fluorescein (CLF) (BD Biosciences) for 30 min. The cells were washed with culture medium, and then observed by fluorescence microscope. To inhibit the function of BSEP, the cells were pretreated with Cyclosporin A 24 h before of the CLF treatment.

2.10. Assay for CYP activity and CYP induction

To measure the cytochrome P450 2C9 and 3A4 activity of the cells, we performed lytic assays by using a P450-GloTM CYP2C9 (catalog number; V8791) and

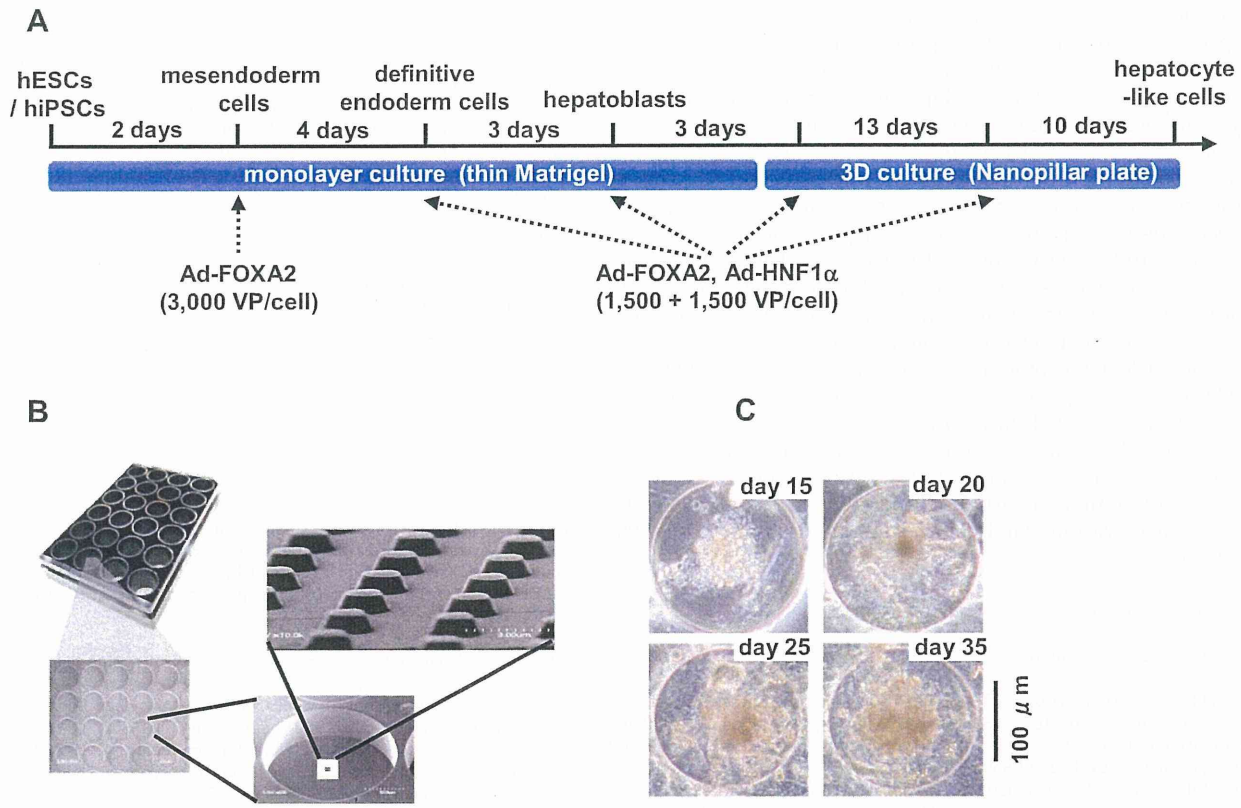

Fig. 1. Hepatocyte-like cells were differentiated from hESCs/hiPSCs by using Nanopillar Plate. (A) The procedure for differentiation of hESCs into 3D ES/iPS-hepa via mesendoderm cells, definitive endoderm cells, and hepatoblasts is presented schematically. In the differentiation, not only the addition of growth factors but also stage-specific transient transduction of both FOXA2- and HNF1α-expressing Ad vector (Ad-FOXA2 and Ad-HNF1α, respectively) was performed. The cellular differentiation procedure is described in detail in the materials and methods section. (B) Photograph display of a 24-well format Nanopillar Plate and its microstructural appearances of the hole and pillar structure. (C) Phase-contrast micrographs of the hESC-hepa spheroids on the Nanopillar Plate are shown. Scale bar represents 100 μm.

3A4 (catalog number; V9001) Assay Kit (Promega), respectively. We measured the fluorescence activity with a luminometer (Lumat LB 9507; Berthold) according to the manufacturer's instructions. The CYP activity was normalized with the protein content per well.

To measure CYP2C9 and 3A4 induction potency, the CYP activity was measured by using a P450-GloTM CYP2C9 and 3A4 Assay Kit, respectively. The cells were treated with rifampicin, which is known to induce both CYP2C9 and 3A4, at a final concentration of 10 μM for 48 h. The cells were also treated with Ketoconazole (Sigma) or Sulfaphenazole (Sigma), which are inhibitors for CYP3A4 or 2C9, at a final concentration of 1 μM or 2 μM, respectively, for 48 h. Controls were treated with DMSO (final concentration 0.1%). Inducer compounds were replaced daily.

2.11. Cell viability tests

Cell viability was assessed by the WST-8 assay kit (Dojindo) in Fig. 2D. After treatment with test compounds, such as Acetaminophen (Wako), Allopurinol (Wako), Amiodaron (Sigma), Benzbromarone (Sigma), Clozapine (Wako), Cyclizine (MP bio), Dantrolene (Wako), Desipramine (Wako), Disufliram (Wako), Erythromycin (Wako), Felbamate (Sigma), Flutamide (Wako), Isoniazid (Sigma), Labetalol (Sigma), Lefunomide (Sigma), Maprotiline (Sigma), Nefazodone (Sigma), Nitrofurantoin (Sigma), Sulindac (Wako), Tacrine (Sigma), Tebinafine (Wako), Tolcapone (TRC), Troglitazone (Wako), and Zafirlukast (Cayman) for 24 h, the cell viability was measured. The cell viability of the 3D iPSC-hepa were assessed by WST-8 assay after 24 h exposure to different concentrations of Aflatoxin B1 (Sigma) and Benzbromarone in the presence or absence of the CYP3A4 or 2C9 inhibitor, Ketoconazole (1 μM) or Sulfaphenazole (10 μM), respectively. The control refers to incubations in the absence of test compounds and was considered as 100% viability value. Controls were treated with DMSO (final concentration 0.1%). ATP assay (BioAssay Systems), Alamar Blue assay (Invitrogen), and Crystal Violet (Wako) staining assay were performed according to the manufacturer's instructions.

2.12. Primary human hepatocytes

Three lots of cryopreserved human hepatocytes (lot Hu8072 [CellzDirect], HC2-14, and HC10-101 [Xenotech]) were used. These three lots of crypreserved human hepatocytes were cultured according to our previous report [5].

2.13. Statistical analysis

Statistical analysis was performed using the unpaired two-tailed Student's *t*-test. All data are represented as means ± SD ($n = 3$).

3. Results

The 3D ES/iPS-hepa were generated from hESCs/hiPSCs as shown in Fig. 1A. Hepatocyte differentiation of hESCs/hiPSCs was efficiently promoted by stage-specific transient transduction of FOXA2 and HNF1α in addition to the treatment with appropriate soluble factors (growth factors and cytokines) [6]. On day 11, the hESC-derived cells were seeded at 2.5×10^5 cells/cm^2 (Fig. S1) on Nanopillar Plate (Fig. 1B), in hepatocyte culture medium (Fig. S2) to promote hepatocyte maturation. In addition, Matrigel was overlaid on the 3D ES-hepa to promote further hepatocyte maturation. The 3D ES-hepa with compact morphology that were adhesive to the substratum and had an optimal size (approximately 100 μm in diameter) were formed by using the Nanopillar Plate (Fig. 1C). The spheroids seem to be stable because they could be cultured for more than 20 days. We have confirmed that more than 90% of the cells that constitute the spheroids were alive, indicating that the necrotic centers are absent.

To investigate whether or not a 3D spheroid culture could promote hepatocyte maturation of the hepatocyte-like cells, various hepatocyte characteristics of the 3D ES/iPS-hepa were compared with those of the monolayer-cultured hESC- or hiPSC-derived hepatocyte-like cells (mono ES-hepa or mono iPS-hepa). The gene expression level of *ALB* peaked on day 20 in the mono ES-hepa, and then it was dramatically decreased after day 25 (Fig. 2A). In contrast, the gene expression level of *ALB* was

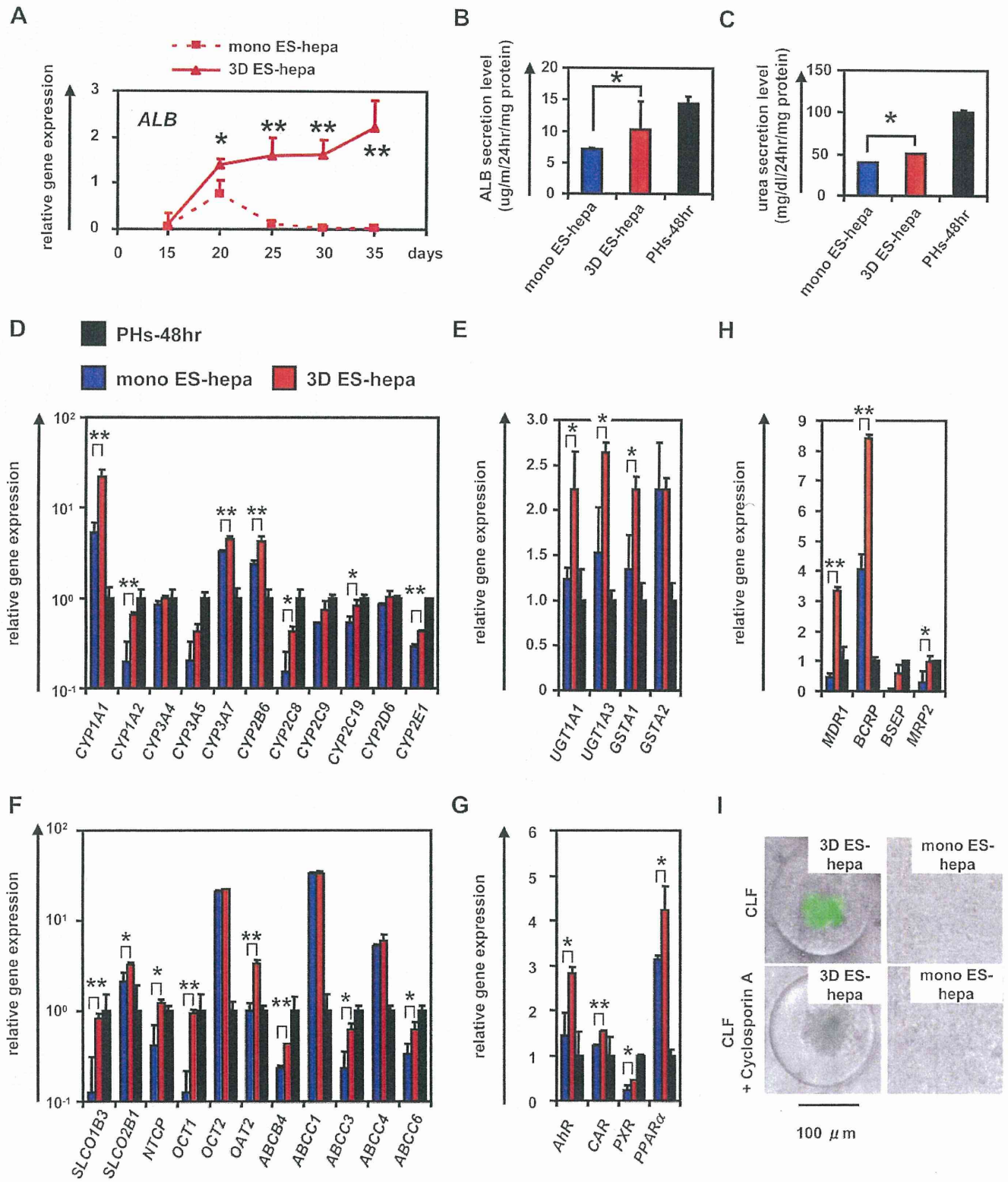

Fig. 2. Hepatocyte functions in hESC-derived hepatocyte-like cells were enhanced by using Nanopillar Plate. (A) The gene expression levels of *ALB* were measured by real-time RT-PCR on day 15, 20, 25, 30, and 35. On the *y* axis, the gene expression levels in PHs (three lots of PHs were used in all studies), which were cultured for 48 h after plating (PHs-48hr), were taken as 1.0. (B, C) The amount of ALB (B) and urea (C) secretion were examined in the mono ES-hepa (day 20), the 3D ES-hepa (day 35), and PHs-48hr. (D–H) The gene expression levels of CYP enzymes (D), conjugating enzymes (E), hepatic transporters (F), hepatic nuclear receptors (G), and bile canaliculi transporters (H) were examined by real-time RT-PCR in the mono ES-hepa, the 3D ES-hepa, and PHs-48hr. On the *y* axis, the expression levels in PHs-48hr were taken as 1.0. (I) The ability of bile acid uptake and efflux was examined in the mono ES-hepa and 3D ES-hepa. Choly-lysyl-fluorescein (CLF) (5 μM) was used for the observation of bile canaliculi uptake and efflux. To inhibit transportation by BSEP, the cells were pretreated with 1 μM Cyclosporin A. $^{*}P < 0.05$; $^{**}P < 0.01$.

moderately increased in the 3D ES-hepa until day 35 (Fig. 2A). These results suggest that the hepatocyte functions of the 3D ES-hepa are sustained for more than 2 weeks on the Nanopillar Plate, although those of the mono ES-hepa are rapidly devitalized (Fig. 2A and Fig. S4). Other hepatocyte characteristics, such as ability of ALB and urea secretion and gene expression levels of hepatocyte-related markers in the 3D ES-hepa were compared with those of the mono ES-hepa (Fig. 2B–H). Because the gene expression level of *ALB* in the 3D ES-hepa was the highest on day 35 and that in mono ES-hepa was the highest on day 20, various hepatocyte characteristics were compared on day 35 or day 20, respectively. The amount of ALB (Fig. 2B) and urea (Fig. 2C) secretion in the 3D ES-hepa was higher than those of the mono ES-hepa. The gene expression levels of CYP enzymes (Fig. 2D), conjugating enzymes (Fig. 2E), hepatic transporters (Fig. 2F), hepatic nuclear receptors (Fig. 2G), and hepatic transcription factors (Fig. S5) in the 3D ES-hepa were higher than those in the mono ES-hepa. The expression levels of most of the genes in the 3D ES-hepa were higher than those in the mono ES-hepa. Because the previous study [11] showed that hepatocyte spheroids expressed hepatocyte transporters similar to those of the bile canaliculi in native liver tissue, the gene expression levels of bile canaliculi transporters (Fig. 2H), as well as the ability of bile acid uptake and efflux, (Fig. 2I) were examined in the 3D ES-hepa. The gene expression levels of bile canaliculi transporters were increased in the 3D ES-hepa compared with those of mono ES-hepa and PHs (Fig. 2H). The bile canaliculi formation was visualized by BSEP fluorescent substrate: Cholyl-lysyl-fluorescein (CLF), which is inhibited by BSEP

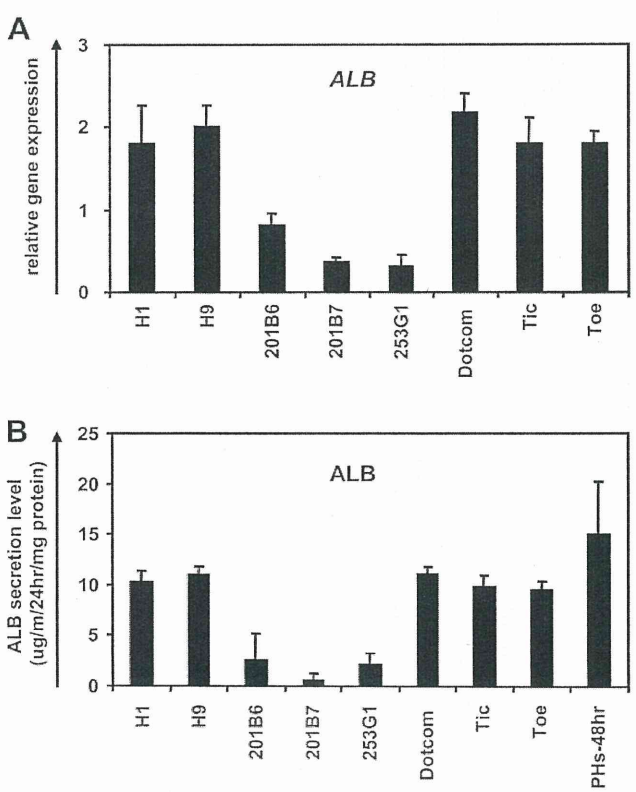

Fig. 3. Comparison of the hepatic differentiation capacities of various hESC and hiPSC lines hESCs (H1 and H9) and hiPSCs (201B6, 201B7, 253G1, Dotcom, Tic, and Toe) were differentiated into the 3D ES/iPS-hepa as described in Fig. 1A. (A) On day 20, the gene expression level of *ALB* was examined by real-time RT-PCR. On the *y* axis, the gene expression level of *ALB* in PHs-48hr was taken as 1.0. (B) On day 20, the amount of ALB secretion was examined by ELISA. The amount of ALB secretion was calculated according to each standard followed by normalization to the protein content per well.

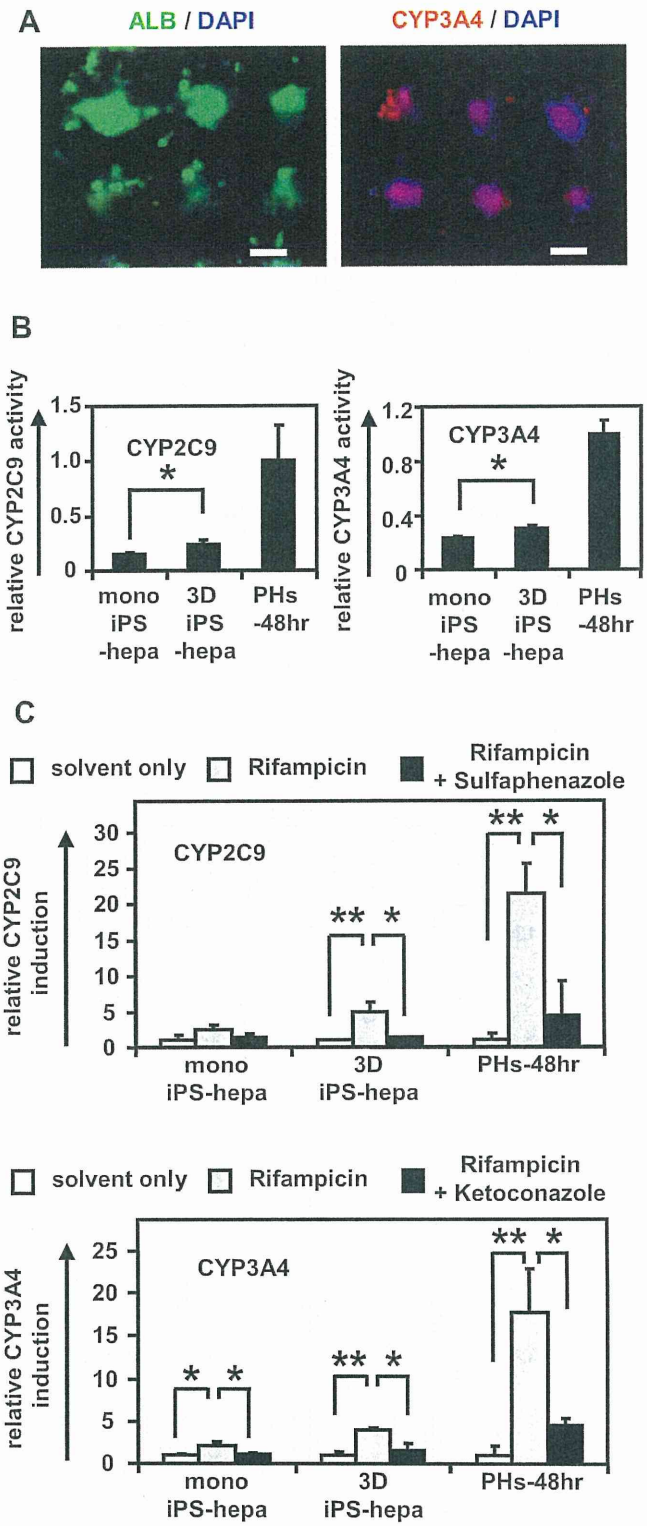

Fig. 4. Drug metabolism capacity and CYP induction potency were examined in the 3D iPS-hepa. (A) The 3D iPS-hepa (day 35) were subjected to immunostaining with anti-ALB (green) or CYP3A4 (red) antibodies. Nuclei were counterstained with DAPI (blue). Scale bar represents 100 μm. (B) The CYP activity was measured in the mono iPS-hepa (day 20), the 3D iPS-hepa (day 35), and PHs-48hr. On the *y* axis, the CYP activity in PHs-48hr was taken as 1.0. (C) Induction of CYP2C9 (left) or CYP3A4 (right) by DMSO (solvent only; white bar), Rifampicin (gray bar), or rifampicin and CYP inhibitor (Sulfaphenazole or Ketoconazole, black bar) in the mono iPS-hepa, the 3D iPS-hepa, and PHs-48hr. On the *y* axis, the CYP activity of the cells that have been cultured in DMSO-containing medium was taken as 1.0. $^{*}P < 0.05$; $^{**}P < 0.01$.

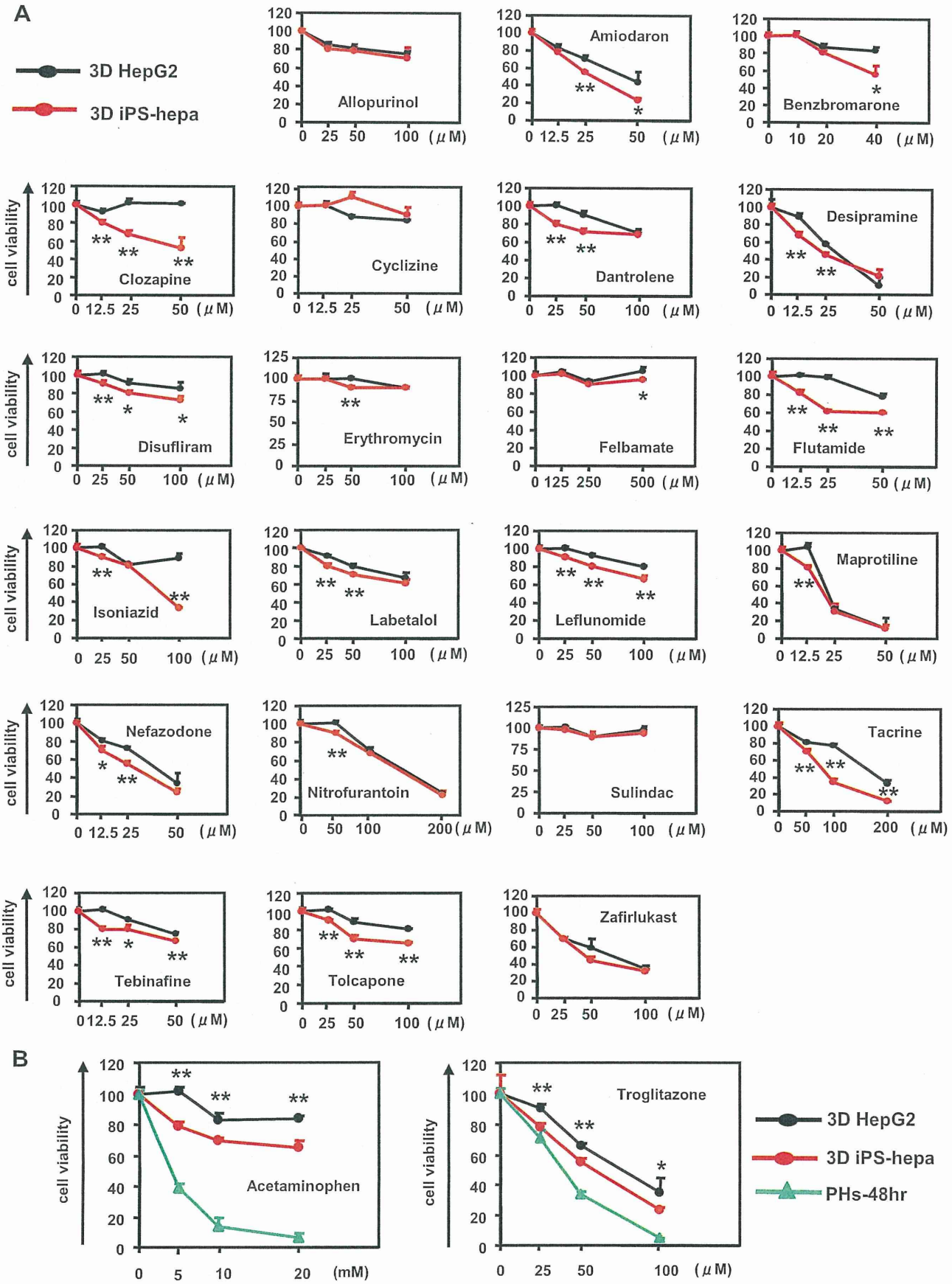
A
3D HepG2
3D iPS-hepa
cell viability
Allopurinol
Amiodaron
Benzbromarone
Clozapine
Cyclizine
Dantrolene
Desipramine
Disufliram
Erythromycin
Felbamate
Flutamide
Isoniazid
Labetalol
Leflunomide
Maprotiline
Nefazodone
Nitrofurantoin
Sulindac
Tacrine
Tebinafine
Tolcapone
Zafirlukast
B
Acetaminophen
Troglitazone
3D HepG2
3D iPS-hepa
PHs-48hr
(μM)
(mM)

inhibitor Cyclosporin A [22,23]. More CLF was accumulated in the 3D ES-hepa than in the mono ES-hepa (Fig. 2I *upper panel*). Moreover, CLF accumulation was inhibited by Cyclosporin A treatment only in the 3D ES-hepa (Fig. 2I *lower panel*), demonstrating that the functionality of BSEP transporter in 3D ES-hepa was greater than that in mono ES-hepa. These results suggested that hepatocyte maturation was promoted by the culture on the Nanopillar Plate. It is likely that, compared to the monolayer culture condition, the 3D spheroid-culture condition is more similar to the *in vivo* condition.

It is important to select an hESC/hiPSC line that has a strong ability to differentiate into hepatocyte-like cells in the case of medical applications such as drug screening. In this study, two hESC lines and six hiPSC lines were differentiated into the hepatocyte-like cells, and then their gene expression levels of *ALB* (Fig. 3A) and ALB secretion levels (Fig. 3B) were compared. These results suggest that the iPSC line, Dotcom, was the suitable cell line for hepatocyte maturation. Therefore, the iPSC line, Dotcom, was used to examine the possibility of the 3D iPS-hepa for drug screening. The drug metabolism capacity and the CYP induction potency of the 3D iPS-hepa were compared with those of the mono iPS-hepa. We confirmed the expression of ALB and CYP3A4 protein in the 3D ES-hepa (Fig. 4A). The activity levels of CYP enzymes in the 3D iPS-hepa were measured according to the metabolism of the CYP2C9 or CYP3A4 substrates (Fig. 4B); the levels were higher than those of the mono iPS-hepa (Fig. 4B). We further tested the induction of CYP2C9 and CYP3A4 by chemical stimulation (rifampicin was used as a CYP2C9 or CYP3A4 inducer). Compared with mono iPS-hepa, the 3D iPS-hepa produced more metabolites in response to chemical stimulation (Fig. 4C). In addition, the CYP induction was inhibited by using CYP2C9 or CYP3A4 inhibitor (Sulfaphenazole or Ketoconazole, respectively). These results indicated that drug metabolism capacity and CYP induction potency in 3D iPS-hepa were higher than those in mono iPS-hepa.

Many researchers have tried to predict the drug-induced cytotoxicity *in vitro* using hepatocarcinoma-derived cells such as HepG2 cells [24,25]. HepG2 cells are less expensive than PHs and the reproducible experiments are easier to perform than they are with PHs, although 30% of the compounds were incorrectly classified as nontoxic [24,25]. To overcome these problems, hESC/hiPSC-derived hepatocyte-like cells are expected to be used to predict drug-induced cytotoxicity. To examine its applicability to drug screening, the 3D iPS-hepa were treated with various drugs, that cause hepatotoxicity. WST-8 assay was performed to evaluate cell viability (Fig. S6). The susceptibility of the 3D iPS-hepa to most of the hepatotoxic drugs was higher than that of the mono iPS-hepa (Fig. S7). Compared to the mono iPS-hepa, the 3D iPS-hepa were more suitable tools for drug screening. Next, the susceptibility of the 3D iPS-hepa to the hepatotoxic drugs was compared with that of the 3D spheroid cultured HepG2 cells (3D HepG2; the hepatocyte functions of 3D HepG2 cells are higher than those of monolayer cultured HepG2 cells [Fig. S8]). With most of the drugs, the cell viability of the 3D iPS-hepa was lower than that of the 3D HepG2 (Fig. 5A). These results indicated that the 3D iPS-hepa are more valuable tools for drug screening than the 3D HepG2. However, the susceptibility of the 3D iPS-hepa to Acetaminophen and Troglitazone was lower than that of the PHs which were cultured for 48 h after the cells were plated (Fig. 5B). These results might be due to the lower activity levels of CYPs in 3D iPS-hepa as compared as those in PHs. Taken together, 3D iPS-hepa are more valuable tools for drug screening than the 3D HepG2, although further maturation of 3D iPS-hepa is still required for 3D iPS-hepa to be an alternative cell source of PHs in the drug screening.

To examine whether drug-induced cytotoxicity is caused by CYP metabolites in 3D iPS-hepa, Aflatoxin B1 (mainly metabolized by CYP3A4 [26]) and Benzbromarone (mainly metabolized by CYP2C9 [27]) were treated in the presence or absence of a CYP3A4 and a 2C9 inhibitor, Ketoconazole and Sulfaphenazole, respectively (Fig. 6). The cell viability of 3D iPS-hepa was partially rescued by treatment with the CYP inhibitor. These results indicated that drug-induced cytotoxicity was caused by CYP metabolites of Aflatoxin B1 and Benzbromarone.

4. Discussion

Recently, it has been expected that human pluripotent stem cells and their derivatives, including hepatocyte-like cells, will be utilized in applications for the safety assessment of drugs. We have previously reported that combinational overexpression of SOX17, HEX, and HNF4α, or combinational overexpression of FOXA2 and HNF1α could promote hepatocyte differentiation [5,6]. However, the drug metabolism capacity of the hepatocyte-like cells generated by our previous protocol was still lower than that of primary human hepatocytes [6]. To generate more matured hepatocyte-like cells as compared with our previous protocol, we established a hepatocyte differentiation method employing not only stage-specific transient overexpression of hepatocyte-related transcription factors but also a 3D culture systems using a Nanopillar Plate, was established. Although the use of hepatocyte-like cells generated from hESCs/hiPSCs in application for drug toxicity testing has begun to be focused, to the best of our knowledge, there have been few studies that have investigated whether hepatocyte-like cells could predict many kinds of drug-induced toxicity.

3D culture spheroids were generated from hESCs/hiPSCs by using a Nanopillar Plate. The diameter of the spheroids was approximately 100 μm on day 35 of differentiation (Fig. 1C). Because it is known that the no-oxygen limitation would take place in spheroids up to 100 μm in diameter [28], the size of the spheroid might be important to generate spheroids with high viability. A Nanopillar Plate has a potential to regulate the spheroid diameter simply by culturing under optimized seeding condition, on its suitably designed pillar and hole structure [11]. Therefore, a Nanopillar Plate would be a suitable environment for the generation of 3D ES/iPS-hepa that show high viability and possess high level of hepatocellular functions.

The levels of many hepatocyte functions, such as ALB secretion ability (Fig. 2B), urea secretion ability (Fig. 2C), hepatocyte-related gene expressions (Fig. 2D–H), drug metabolism capacity (Fig. 4B), and CYP induction potency (Fig. 4C), of 3D ES/iPS-hepa were higher than those of mono ES/iPS-hepa. This might have been because the structural and functional polarity, which can be seen in the naïve environment of hepatocytes, of the hepatocyte-like cells was configured by a 3D culturing condition. Previous studies have shown that a 3D culture condition is suitable to maintain the hepatic characteristics of the isolated hepatocytes because this condition mimic *in vivo* environment [29,30]. These facts indicated that the 3D culture condition is a more suitable condition for the hepatocyte-like cells than the monolayer culture condition.

Two hES cell lines and six hiPS cell lines were differentiated into the hepatocyte-like cells in this study. The hiPS cell line, Dotcom, seemed to be a suitable cell line for hepatic differentiation (Fig. 3). Because the hepatic differentiation propensity differs among the

Fig. 5. The possibility of applying 3D iPS-hepa to drug testing was examined. (A) The cell viability of the 3D HepG2 (black) and 3D iPSC-hepa (red) were assessed by WST-8 assay after 24 h exposure to different concentrations of 22 test compounds. (B) The cell viability of the 3D HepG2 (black), 3D iPSC-hepa (red), and PHs-48hr (green) were assessed by WST-8 assay after 24 h exposure to different concentrations of Acetaminophen and Troglitazone. Cell viability is expressed as a percentage of cells treated with solvent only. $^{*}P < 0.05$; $^{**}P < 0.01$.

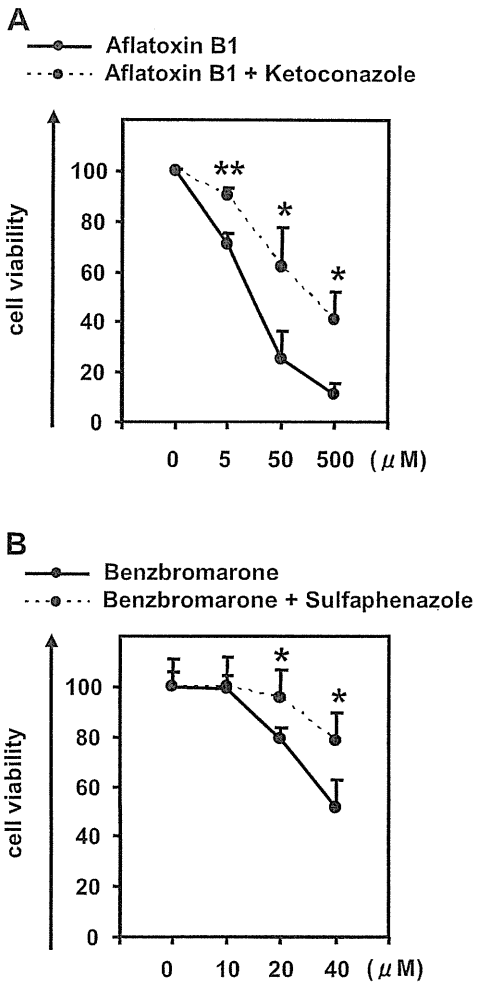

Fig. 6. Drug-induced cytotoxicity in the 3D iPS-hepa is mediated by cytochrome P450. (A, B) The cell viability of the 3D iPSC-hepa was assessed by WST-8 assay after 24 h exposure to different concentrations of (A) Aflatoxin B1 and (B) Benzbromarone in the presence or absence of the CYP3A4 or 2C9 inhibitor, Ketoconazole or Sulfaphenazole, respectively. Cell viability was expressed as the percentage of cells treated with solvent only. $^{*}P < 0.05$; $^{**}P < 0.01$.

hES/hiPS cell lines, it would be important to select an appropriate cell line for medical applications such as drug screening. However, the dominant reason for this hepatic differentiation propensity is not been well known. It would be interesting study to elucidate the mechanism of this propensity.

Although the drug metabolism capacity and CYP induction potency of 3D iPS-hepa were higher than those of mono iPS-hepa (Fig. 4B and C), they were still lower than those of primary human hepatocytes. The hepatic nuclear factors are known to be key molecules in the CYP induction of hepatocytes [30]. Therefore, overexpression of hepatic nuclear factors, which are not abundantly expressed in the hepatocyte-like cells (such as *PXR*), might upregulate the CYP induction potency of the hepatocyte-like cells.

3D iPS-hepa were more sensitive for detection of the drug-induced cytotoxicity than HepG2 cells that are widely used to predict hepatotoxicity [31,32] (Fig. 5). In addition, the decrease of cell viability, which was caused by hepatotoxic drugs, of 3D iPS-hepa was partially rescued by treatment with a CYP inhibitor (Fig. 6). These data suggest that the hepatocyte-like cells could detect the toxicity of the reactive metabolites that were generated by drug metabolizing enzymes such as CYP enzymes. Because in many cases, drug-induced hepatotoxicity is caused by the reactive metabolites produced by drug metabolizing enzymes [33], our finding that the hepatocyte-like cells could detect the toxicity of reactive metabolites should be of great potential for toxicological screening. Moreover, it might be possible to predict idiosyncratic liver toxicity by using hepatocyte-like cells generated from hiPSCs that were established from a patient with a rare CYP polymorphism. However, some compounds did not show any cytotoxicity (such as Cyclizine, Felbamate, and Sulindac) (Fig. 5). To apply the hepatocyte-like cells for wide-spread drug screening, generation of the hepatocyte-like cells are required to detect hepatotoxity in more sensitive manner. Previous studies showed that the depletion of conjugating enzymes [32] or knockdown of Nrf2 [34] expression are useful to upregulate the sensitivity to hepatotoxic drugs. Therefore, these approaches would be useful to generate more sensitive hepatocytes to toxic drugs.

5. Conclusions

In this study, we established the efficient hepatocyte differentiation method which employs not only stage-specific transient overexpression of hepatocyte-related transcription factors but also 3D spheroid culture systems by using Nanopillar Plate. To the best of our knowledge, this is the first study in which the hepatocyte-like cells, having enough hepatocyte functions, mediate drug-induced cytotoxicity against many compounds. Our hepatocyte-like cells differentiated from hESCs or hiPSCs have potential to be applied in drug toxicity testing.

Acknowledgments

We thank Misae Nishijima and Hiroko Matsumura for their excellent technical support. HM, KK, MKF, and TH were supported by grants from the Ministry of Health, Labor, and Welfare of Japan. HM was also supported by Japan Research foundation For Clinical Pharmacology, and The Uehara Memorial Foundation. MKF was also supported by Japan Society for the Promotion of Science Grant-in-Aid for Scientific Research. FS was supported by Program for Promotion of Fundamental Studies in Health Sciences of the National Institute of Biomedical Innovation (NIBIO). We thank Hiromu Yamada (NIBIO) for helpful discussion.

Appendix A. Supplementary data

Supplementary data related to this article can be found at http://dx.doi.org/10.1016/j.biomaterials.2012.11.029.

References

[1] Thomson JA, Itskovitz-Eldor J, Shapiro SS, Waknitz MA, Swiergiel JJ, Marshall VS, et al. Embryonic stem cell lines derived from human blastocysts. Science 1998;282:1145–7.
[2] Takahashi K, Tanabe K, Ohnuki M, Narita M, Ichisaka T, Tomoda K, et al. Induction of pluripotent stem cells from adult human fibroblasts by defined factors. Cell 2007;131:861–72.
[3] Inamura M, Kawabata K, Takayama K, Tashiro K, Sakurai F, Katayama K, et al. Efficient generation of hepatoblasts from human ES cells and iPS cells by transient overexpression of homeobox gene HEX. Mol Ther 2011;19:400–7.
[4] Takayama K, Inamura M, Kawabata K, Tashiro K, Katayama K, Sakurai F, et al. Efficient and directive generation of two distinct endoderm lineages from human ESCs and iPSCs by differentiation stage-specific SOX17 transduction. PLoS One 2011;6:e21780.
[5] Takayama K, Inamura M, Kawabata K, Katayama K, Higuchi M, Tashiro K, et al. Efficient generation of functional hepatocytes from human embryonic stem cells and induced pluripotent stem cells by HNF4alpha transduction. Mol Ther 2012;20:127–37.
[6] Takayama K, Inamura M, Kawabata K, Sugawara M, Kikuchi K, Higuchi M, et al. Generation of metabolically functioning hepatocytes from human pluripotent stem cells by FOXA2 and HNF1alpha transduction. J Hepatol 2012;57:628–36.
[7] Ramasamy TS, Yu JS, Selden C, Hodgson H, Cui W. Application of three-dimensional culture conditions to human embryonic stem cell-derived

definitive endoderm cells enhances hepatocyte differentiation and functionality. Tissue Eng Part A. http://dx.doi.org/10.1089/ten.tea.2012.0190. Available from URL: http://www.ncbi.nlm.nih.gov/pubmed/23003670; 2012.
[8] Nagamoto Y, Tashiro K, Takayama K, Ohashi K, Kawabata K, Sakurai F, et al. The promotion of hepatic maturation of human pluripotent stem cells in 3D co-culture using type I collagen and Swiss 3T3 cell sheets. Biomaterials 2012;33:4526–34.
[9] Meng Q, Haque A, Hexig B, Akaike T. The differentiation and isolation of mouse embryonic stem cells toward hepatocytes using galactose-carrying substrata. Biomaterials 2012;33:1414–27.
[10] Shiraki N, Yamazoe T, Qin Z, Ohgomori K, Mochitate K, Kume K, et al. Efficient differentiation of embryonic stem cells into hepatic cells in vitro using a feeder-free basement membrane substratum. PLoS One 2011;6:e24228.
[11] Takahashi R, Sonoda H, Tabata Y, Hisada A. Formation of hepatocyte spheroids with structural polarity and functional bile canaliculi using nanopillar sheets. Tissue Eng Part A 2010;16:1983–95.
[12] Tong JZ, Sarrazin S, Cassio D, Gauthier F, Alvarez F. Application of spheroid culture to human hepatocytes and maintenance of their differentiation. Biol Cell 1994;81:77–81.
[13] Bi YA, Kazolias D, Duignan DB. Use of cryopreserved human hepatocytes in sandwich culture to measure hepatobiliary transport. Drug Metab Dispos 2006;34:1658–65.
[14] Makino H, Toyoda M, Matsumoto K, Saito H, Nishino K, Fukawatase Y, et al. Mesenchymal to embryonic incomplete transition of human cells by chimeric OCT4/3 (POU5F1) with physiological co-activator EWS. Exp Cell Res 2009;315:2727–40.
[15] Nagata S, Toyoda M, Yamaguchi S, Hirano K, Makino H, Nishino K, et al. Efficient reprogramming of human and mouse primary extra-embryonic cells to pluripotent stem cells. Genes Cells 2009;14:1395–404.
[16] Furue MK, Na J, Jackson JP, Okamoto T, Jones M, Baker D, et al. Heparin promotes the growth of human embryonic stem cells in a defined serum-free medium. Proc Natl Acad Sci U S A 2008;105:13409–14.
[17] Kawabata K, Inamura M, Mizuguchi H. Efficient hepatic differentiation from human iPS cells by gene transfer. Methods Mol Biol 2012;826:115–24.
[18] Mizuguchi H, Kay MA. Efficient construction of a recombinant adenovirus vector by an improved in vitro ligation method. Hum Gene Ther 1998;9:2577–83.
[19] Mizuguchi H, Kay MA. A simple method for constructing E1- and E1/E4-deleted recombinant adenoviral vectors. Hum Gene Ther 1999;10:2013–7.
[20] Tashiro K, Kawabata K, Sakurai H, Kurachi S, Sakurai F, Yamanishi K, et al. Efficient adenovirus vector-mediated PPAR gamma gene transfer into mouse embryoid bodies promotes adipocyte differentiation. J Gene Med 2008;10:498–507.
[21] Maizel Jr JV, White DO, Scharff MD. The polypeptides of adenovirus. I. Evidence for multiple protein components in the virion and a comparison of types 2, 7A, and 12. Virology 1968;36:115–25.
[22] Yasumiba S, Tazuma S, Ochi H, Chayama K, Kajiyama G. Cyclosporin A reduces canalicular membrane fluidity and regulates transporter function in rats. Biochem J 2001;354:591–6.
[23] Roman ID, Fernandez-Moreno MD, Fueyo JA, Roma MG, Coleman R. Cyclosporin A induced internalization of the bile salt export pump in isolated rat hepatocyte couplets. Toxicol Sci 2003;71:276–81.
[24] Rodriguez-Antona C, Donato MT, Boobis A, Edwards RJ, Watts PS, Castell JV, et al. Cytochrome P450 expression in human hepatocytes and hepatoma cell lines: molecular mechanisms that determine lower expression in cultured cells. Xenobiotica 2002;32:505–20.
[25] Hewitt NJ, Hewitt P. Phase I and II enzyme characterization of two sources of HepG2 cell lines. Xenobiotica 2004;34:243–56.
[26] Gallagher EP, Kunze KL, Stapleton PL, Eaton DL. The kinetics of aflatoxin B1 oxidation by human cDNA-expressed and human liver microsomal cytochromes P450 1A2 and 3A4. Toxicol Appl Pharmacol 1996;141:595–606.
[27] Lee MH, Graham GG, Williams KM, Day RO. A benefit-risk assessment of benzbromarone in the treatment of gout. Was its withdrawal from the market in the best interest of patients? Drug Saf 2008;31:643–65.
[28] Glicklis R, Merchuk JC, Cohen S. Modeling mass transfer in hepatocyte spheroids via cell viability, spheroid size, and hepatocellular functions. Biotechnol Bioeng 2004;86:672–80.
[29] Kim K, Ohashi K, Utoh R, Kano K, Okano T. Preserved liver-specific functions of hepatocytes in 3D co-culture with endothelial cell sheets. Biomaterials 2012;33:1406–13.
[30] Khetani SR, Bhatia SN. Microscale culture of human liver cells for drug development. Nat Biotechnol 2008;26:120–6.
[31] Iwamura A, Fukami T, Hosomi H, Nakajima M, Yokoi T. CYP2C9-mediated metabolic activation of losartan detected by a highly sensitive cell-based screening assay. Drug Metab Dispos 2011;39:838–46.
[32] Hosomi H, Akai S, Minami K, Yoshikawa Y, Fukami T, Nakajima M, et al. An in vitro drug-induced hepatotoxicity screening system using CYP3A4-expressing and gamma-glutamylcysteine synthetase knockdown cells. Toxicol In Vitro 2010;24:1032–8.
[33] Guengerich FP, MacDonald JS. Applying mechanisms of chemical toxicity to predict drug safety. Chem Res Toxicol 2007;20:344–69.
[34] Hosomi H, Fukami T, Iwamura A, Nakajima M, Yokoi T. Development of a highly sensitive cytotoxicity assay system for CYP3A4-mediated metabolic activation. Drug Metab Dispos 2011;39:1388–95.

Research Article

EASL EUROPEAN ASSOCIATION FOR THE STUDY OF THE LIVER | JOURNAL OF HEPATOLOGY

Generation of metabolically functioning hepatocytes from human pluripotent stem cells by FOXA2 and HNF1α transduction

Kazuo Takayama[1,2], Mitsuru Inamura[1,2], Kenji Kawabata[2,3], Michiko Sugawara[4], Kiyomi Kikuchi[4], Maiko Higuchi[2], Yasuhito Nagamoto[1,2], Hitoshi Watanabe[1,2], Katsuhisa Tashiro[2], Fuminori Sakurai[1], Takao Hayakawa[5,6], Miho Kusuda Furue[7,8], Hiroyuki Mizuguchi[1,2,9,*]

[1]*Laboratory of Biochemistry and Molecular Biology, Graduate School of Pharmaceutical Sciences, Osaka University, Osaka 565-0871, Japan;* [2]*Laboratory of Stem Cell Regulation, National Institute of Biomedical Innovation, Osaka 567-0085, Japan;* [3]*Laboratory of Biomedical Innovation, Graduate School of Pharmaceutical Sciences, Osaka University, Osaka 565-0871, Japan;* [4]*Tsukuba Laboratories, Eisai Co., Ltd., Ibaraki 300-2635, Japan;* [5]*Pharmaceutics and Medical Devices Agency, Tokyo 100-0013, Japan;* [6]*Pharmaceutical Research and Technology Institute, Kinki University, Osaka 577-8502, Japan;* [7]*Laboratory of Cell Cultures, Department of Disease Bioresources Research, National Institute of Biomedical Innovation, Osaka 567-0085, Japan;* [8]*Laboratory of Cell Processing, Institute for Frontier Medical Sciences, Kyoto University, Kyoto 606-8507, Japan;* [9]*The Center for Advanced Medical Engineering and Informatics, Osaka University, Osaka 565-0871, Japan*

Background & Aims: Hepatocyte-like cells differentiated from human embryonic stem cells (hESCs) and induced pluripotent stem cells (hiPSCs) can be utilized as a tool for screening for hepatotoxicity in the early phase of pharmaceutical development. We have recently reported that hepatic differentiation is promoted by sequential transduction of SOX17, HEX, and HNF4α into hESC- or hiPSC-derived cells, but further maturation of hepatocyte-like cells is required for widespread use of drug screening.
Methods: To screen for hepatic differentiation-promoting factors, we tested the seven candidate genes related to liver development.
Results: The combination of two transcription factors, FOXA2 and HNF1α, promoted efficient hepatic differentiation from hESCs and hiPSCs. The expression profile of hepatocyte-related genes (such as genes encoding cytochrome P450 enzymes, conjugating enzymes, hepatic transporters, and hepatic nuclear receptors) achieved with FOXA2 and HNF1α transduction was comparable to that obtained in primary human hepatocytes. The hepatocyte-like cells generated by FOXA2 and HNF1α transduction exerted various hepatocyte functions including albumin and urea secretion, and the uptake of indocyanine green and low density lipoprotein. Moreover, these cells had the capacity to metabolize all nine tested drugs and were successfully employed to evaluate drug-induced cytotoxicity.
Conclusions: Our method employing the transduction of FOXA2 and HNF1α represents a useful tool for the efficient generation of metabolically functional hepatocytes from hESCs and hiPSCs, and the screening of drug-induced cytotoxicity.

Keywords: FOXA2; HNF1α; Hepatocytes; Adenovirus; Drug screening; Drug metabolism; hESCs; hiPSCs.
Received 14 November 2011; received in revised form 31 March 2012; accepted 4 April 2012; available online 29 May 2012
* Corresponding author. Address: Laboratory of Biochemistry and Molecular Biology, Graduate School of Pharmaceutical Sciences, Osaka University, 1-6 Yamadaoka, Suita, Osaka 565-0871, Japan. Tel.: +81 6 6879 8185; fax: +81 6 6879 8186.
E-mail address: mizuguch@phs.osaka-u.ac.jp (H. Mizuguchi).

Introduction

Hepatocyte-like cells differentiated from human embryonic stem cells (hESCs) [1] or human induced pluripotent stem cells (hiPSCs) [2] have more advantages than primary human hepatocytes (PHs) for drug screening. While application of PHs in drug screening has been hindered by lack of cellular growth, loss of function, and de-differentiation *in vitro* [3], hESC- or hiPSC-derived hepatocyte-like cells (hESC-hepa or hiPSC-hepa, respectively) have potential to solve these problems.

Hepatic differentiation from hESCs and hiPSCs can be divided into four stages: definitive endoderm (DE) differentiation, hepatic commitment, hepatic expansion, and hepatic maturation. Various growth factors are required to mimic liver development [4] and to promote hepatic differentiation. Previously, we showed that transduction of transcription factors in addition to treatment with optimal growth factors was effective to enhance hepatic differentiation [5–7]. An almost homogeneous hepatocyte population was obtained by sequential transduction of SOX17, HEX, and HNF4α into hESC- or hiPSCs-derived cells [7]. However, further maturation of the hESC-hepa and hiPSC-hepa is required for widespread use of drug screening because the drug metabolism capacity of these cells was not sufficient.

In some previous reports, hESC-hepa and hiPSC-hepa have been characterized for their hepatocyte functions in numerous ways, including functional assessment such as glycogen storage and low density lipoprotein (LDL) uptake [7]. To make a more precise judgment as to whether hESC-hepa and hiPSC-hepa can be applied to drug screening, it is more important to assess cytochrome P450 (CYP) induction potency and drug metabolism capacity rather than general hepatocyte function. Although Duan *et al.* have examined the drug metabolism capacity of hESC-hepa, drug metabolites were measured at 24 or 48 h [8]. To precisely

estimate the drug metabolism capacity, the amount of metabolites must be measured during the time when production of metabolites is linearly detected (generally before 24 h). To the best of our knowledge, there have been few reports that have examined various drugs metabolism capacity of hESC-hepa and hiPSC-hepa in detail.

In the present study, seven candidate genes (*FOXA2*, *HEX*, *HNF1α*, *HNF1β*, *HNF4α*, *HNF6*, and *SOX17*) were transduced into each stage of hepatic differentiation from hESCs by using an adenovirus (Ad) vector to screen for hepatic differentiation-promoting factors. Then, hepatocyte-related gene expression profiles and hepatocyte functions in hESC-hepa and hiPSC-hepa generated by the optimized protocol, were examined to investigate whether these cells have PHs characteristics. We used nine drugs, which are metabolized by various CYP enzymes and UDP-glucuronosyltransferases (UGTs), to determine whether the hESC-hepa and hiPSC-hepa have drug metabolism capacity. Furthermore, hESC-hepa and hiPSC-hepa were examined to determine whether these cells may be applied to evaluate drug-induced cytotoxicity.

Materials and methods

In vitro differentiation

Before the initiation of cellular differentiation, the medium of hESCs and hiPSCs was exchanged for a defined serum-free medium, hESF9, and cultured as previously reported [9]. The differentiation protocol for the induction of DE cells, hepatoblasts, and hepatocytes was based on our previous report with some modifications [5,6]. Briefly, in mesendoderm differentiation, hESCs and hiPSCs were dissociated into single cells by using Accutase (Millipore) and cultured for 2 days on Matrigel (BD biosciences) in differentiation hESF-DIF medium which contains 100 ng/ml Activin A (R&D Systems) and 10 ng/ml bFGF (hESF-DIF medium, Cell Science & Technology Institute; differentiation hESF-DIF medium was supplemented with 10 μg/ml human recombinant insulin, 5 μg/ml human apotransferrin, 10 μM 2-mercaptoethanol, 10 μM ethanolamine, 10 μM sodium selenite, and 0.5 mg/ml bovine serum albumin, all from Sigma). To generate DE cells, mesendoderm cells were transduced with 3000 VP/cell of Ad-FOXA2 for 1.5 h on day 2 and cultured until day 6 on Matrigel in differentiation hESF-DIF medium supplemented with 100 ng/ml Activin A and 10 ng/ml bFGF. For induction of hepatoblasts, the DE cells were transduced with each 1500 VP/cell of Ad-FOXA2 and Ad-HNF1α for 1.5 h on day 6 and cultured for 3 days on Matrigel in hepatocyte culture medium (HCM, Lonza) supplemented with 30 ng/ml bone morphogenetic protein 4 (BMP4, R&D Systems) and 20 ng/ml FGF4 (R&D Systems). In hepatic expansion, the hepatoblasts were transduced with each 1500 VP/cell of Ad-FOXA2 and Ad-HNF1α for 1.5 h on day 9 and cultured for 3 days on Matrigel in HCM supplemented with 10 ng/ml hepatocyte growth factor (HGF), 10 ng/ml FGF1, 10 ng/ml FGF4, and 10 ng/ml FGF10 (all from R&D Systems). In hepatic maturation, cells were cultured for 8 days on Matrigel in L15 medium (Invitrogen) supplemented with 8.3% tryptose phosphate broth (BD biosciences), 10% FBS (Vita), 10 μM hydrocortisone 21-hemisuccinate (Sigma), 1 μM insulin, 25 mM $NaHCO_3$ (Wako), 20 ng/ml HGF, 20 ng/ml Oncostatin M (OsM, R&D systems), and 10^{-6} M Dexamethasone (DEX, Sigma).

Results

Recently, we showed that the sequential transduction of SOX17, HEX, and HNF4α into hESC-derived mesendoderm, DE, and hepatoblasts, respectively, leads to efficient generation of the hESC-hepa [5–7]. In the present study, to further improve the differentiation efficiency towards hepatocytes, we screened for hepatic differentiation-promoting transcription factors. Seven candidate genes involved in liver development were selected. We then examined the function of the hESC-hepa and hiPSC-hepa generated by the optimized protocol for pharmaceutical use in detail.

Efficient hepatic differentiation by Ad-FOXA2 and Ad-HNF1α transduction

To perform efficient DE differentiation, T-positive hESC-derived mesendoderm cells (day 2) (Supplementary Fig. 1) were transduced with Ad vector expressing various transcription factors (Ad-FOXA2, Ad-HEX, Ad-HNF1α, Ad-HNF1β, Ad-HNF4α, Ad-HNF6, and Ad-SOX17 were used in this study). We ascertained the expression of *FOXA2*, *HEX*, *HNF1α*, *HNF1β*, *HNF4α*, *HNF6*, or *SOX17* in Ad-FOXA2-, Ad-HEX-, Ad-HNF1α-, Ad-HNF1β-, Ad-HNF4α-, Ad-HNF6-, or Ad-SOX17-transduced cells, respectively (Supplementary Fig. 2). We also verified that there was no cytotoxicity of the cells transduced with Ad vector until the total amount of Ad vector reached 12,000 VP/cell (Supplementary Fig. 3). Each transcription factor was expressed in hESC-derived mesendoderm cells on day 2 by using Ad vector, and the efficiency of DE differentiation was examined (Fig. 1A). The DE differentiation efficiency based on CXCR4-positive cells was the highest when Ad-SOX17 or Ad-FOXA2 were transduced (Fig. 1B). To investigate the difference between Ad-FOXA2-transduced cells and Ad-SOX17-transduced cells, gene expression levels of markers of undifferentiated cells, mesendoderm cells, DE cells, and extraembryonic endoderm cells were examined (Fig. 1C). The expression levels of extraembryonic endoderm markers of Ad-SOX17-transduced cells were higher than those of Ad-FOXA2-transduced cells. Therefore, we concluded that FOXA2 transduction is suitable for use in selective DE differentiation.

To promote hepatic commitment, various transcription factors were transduced into DE cells and the resulting phenotypes were examined on day 9 (Fig. 1D). Nearly 100% of the population of Ad-FOXA2-transduced cells and Ad-HNF1α-transduced cells was α-fetoprotein (AFP)-positive (Fig. 1E). We expected that hepatic commitment would be further accelerated by combining FOXA2 and HNF1α transduction. The DE cells were transduced with both Ad-FOXA2 and Ad-HNF1α, and then the gene expression levels of *CYP3A7* [10], which is a marker of fetal hepatocytes, were evaluated (Fig. 1F). When both Ad-FOXA2 and Ad-HNF1α were transduced into DE cells, the promotion of hepatic commitment was greater than in Ad-FOXA2-transduced cells or Ad-HNF1α-transduced cells.

To promote hepatic expansion and maturation, we transduced various transcription factors into hepatoblasts on day 9 and 12 and the resulting phenotypes were examined on day 20 (Fig. 1G). We ascertained that the hepatoblast population was efficiently expanded by addition of HGF, FGF1, FGF4, and FGF10 (Supplementary Fig. 4). The hepatic differentiation efficiency based on asialoglycoprotein receptor 1 (ASGR1)-positive cells was measured on day 20, demonstrating that FOXA2, HNF1α, and HNF4α transduction could promote efficient hepatic maturation (Fig. 1H). To investigate the phenotypic difference between Ad-FOXA2-, Ad-HNF1α-, and Ad-HNF4α-transduced cells, gene expression levels of early hepatic markers, mature hepatic markers, and biliary markers were examined (Fig. 1I). Gene expression levels of mature hepatic markers were up-regulated by FOXA2, HNF1α, or HNF4α transduction. FOXA2 transduction strongly upregulated gene expression levels of both early hepatic markers and mature hepatic markers, while HNF1α or HNF4α transduc-

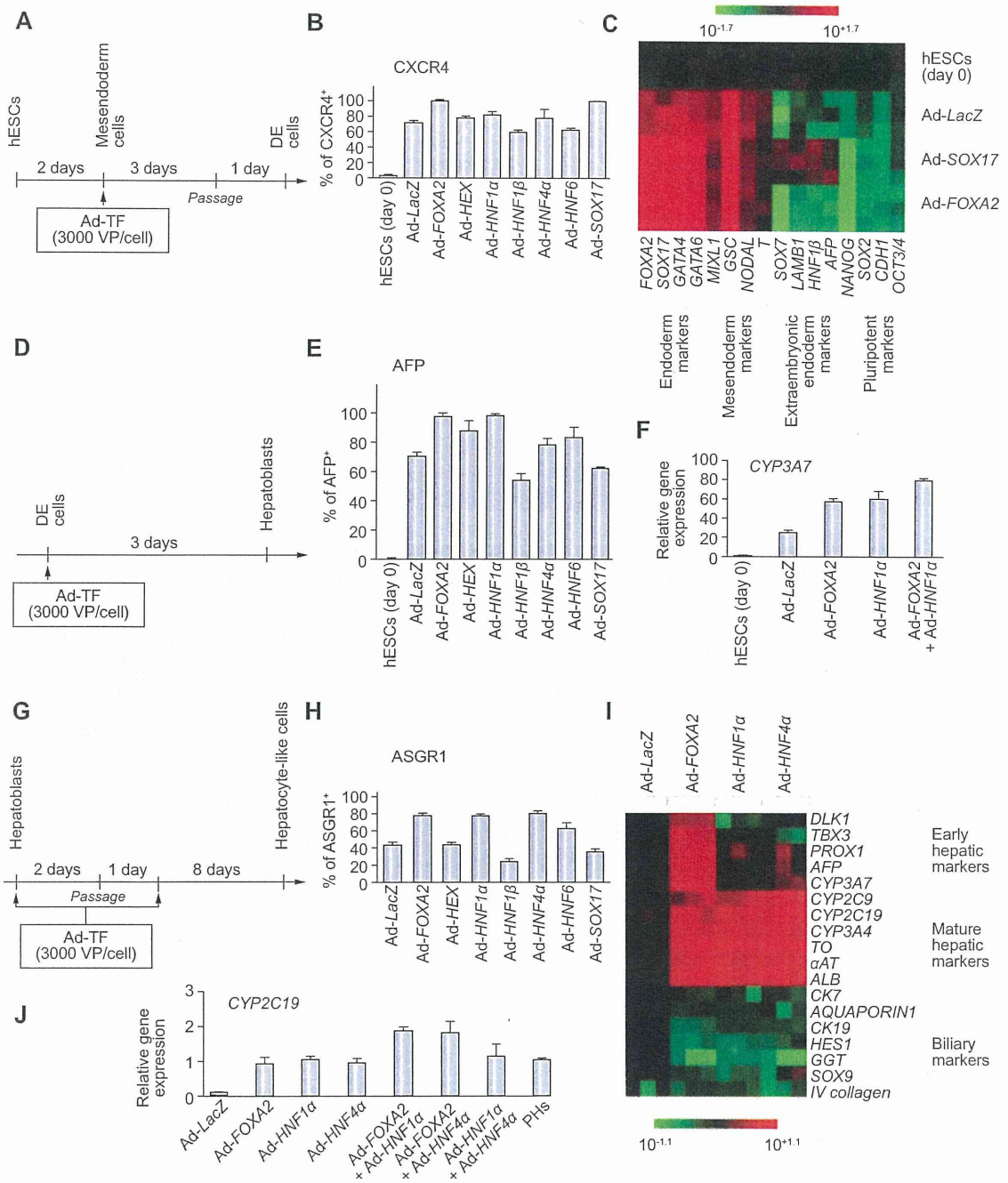

Fig. 1. Efficient hepatic differentiation from hESCs by FOXA2 and HNF1α transduction. (A) The schematic protocol describes the strategy for DE differentiation from hESCs (H9). Mesendoderm cells (day 2) were transduced with 3000 VP/cell of transcription factor (TF)-expressing Ad vector (Ad-TF) for 1.5 h and cultured as described in Fig. 2A. (B) On day 5, the efficiency of DE differentiation was measured by estimating the percentage of CXCR4-positive cells using FACS analysis. (C) The gene expression profiles were examined on day 5. (D) Schematic protocol describing the strategy for hepatoblast differentiation from DE. DE cells (day 6) were transduced with 3000 VP/cell of Ad-TF for 1.5 h and cultured as described in Fig. 2A. (E) On day 9, the efficiency of hepatoblast differentiation was measured by estimating the percentage of AFP-positive